

A COUPLING GENERALIZED MULTISCALE FINITE ELEMENT METHOD FOR COUPLED THERMOMECHANICAL PROBLEMS. *

XIAOFEI GUAN[†], LIJIAN JIANG[‡], YAJUN WANG[‡], AND ZIHAO YANG[¶]

Abstract. It is crucial to build multiscale modeling for the coupling effects between microstructure and the physical mechanisms in multiphysics problems. In the paper, we develop a coupling formulation of the generalized multiscale finite element method (GMsFEM) to solve coupled thermomechanical problems, and it is referred as the coupling generalized multiscale finite element method (CGMsFEM). The approach consists in defining the coupling multiscale basis functions through local coupling spectral problems in each coarse-grid block, which can be solved by a novel design of two relaxation parameters. Compared to the standard GMsFEM, the proposed strategy can not only accurately capture the multiscale coupling correlation effects of multiphysics problems, but also greatly improve the computational efficiency with fewer multiscale basis functions. In addition, the convergence analysis is also established, and the optimal error estimates are derived, where the upper bound of errors is independent of the magnitude of the relaxation coefficient. Several numerical examples for periodic, random microstructure, and random material coefficients are presented to validate the theoretical analysis. The numerical results show that the CGMsFEM approach shows better robustness and efficiency than uncoupled GMsFEM.

Key words. thermomechanical coupled problems, heterogeneous media, generalized multiscale finite element method, coupling multiscale basis functions, error estimates

MSC codes. 65N99, 65N30, 34E13

1. Introduction. Heterogeneous media has been extensively applied to practical engineering, and its physical and mechanical properties across multiple temporal and spatial scales are closely interacted to their underlying microstructure, properties, and compositions etc. Hence, the efficient coupling multiscale modeling is of paramount importance for the performance prediction [11, 12], optimization design [8, 32], and safety assessment [13] of heterogeneous media. In the case of thermomechanical process, except for microscale heterogeneity, microscale thermal expansion properties may also play a significant role at multiple spatial scale. For example, depending on the complex loading conditions (e.g., high stress or extreme temperature environments), damage or cracks may occur due to induced sharp thermal stresses [30], which can be computationally prohibitive. For this reason, efforts should be made to develop more efficient multiscale models and numerical methods to predict the coupled multiphysics behavior of heterogeneous media for engineering practice.

From the first law of thermodynamics and the conservation of momentum, the mathematical modeling of thermomechanical processes can result in coupled partial differential equations (PDEs)[10, 34], which consists of hyperbolic mechanical equations and a parabolic heat transfer equation with coupling each other. Considering the quasi-static case, the existence and uniqueness of the solutions for the coupled PDEs

*Submitted to the editors DATE.

Funding: The work of the first author was supported by the National Science Foundation of China under grant 12271409, the Interdisciplinary Project in Ocean Research of Tongji University and the Fundamental Research Funds for the Central Universities. The work of the second author was supported by the National Science Foundation of China under grant 12271408.

[†]School of Mathematical Sciences, and Key Laboratory of Advanced Civil Engineering Materials of Ministry of Education, Tongji University, Shanghai 200092, China (guanxf@tongji.edu.cn).

[‡]School of Mathematical Sciences, Tongji University, Shanghai 200092, China (ljjiang@tongji.edu.cn, 1910733@tongji.edu.cn).

[¶]School of Mathematics and Statistics, Northwestern Polytechnical University, Xi'an 710072, China (yangzihao@nwpu.edu.cn).

have been analyzed in [33, 39], where the inertia terms of the mechanical parts are ignored. Numerical methods have also been developed with help of the finite element method (FEM), and the convergence analysis and error orders had been obtained in [6, 19]. Numerous studies have focused on the 2D and 3D linear thermomechanical problems [35, 16] and nonlinear thermomechanical problems [38], including coupling effects [18], fracture analysis [14], etc. Here, it should be emphasized that the numerical solution strategies for the mechanical equations are obviously different from that of the poroelastic equations, although they have many similarities in the form of the equations. Furthermore, the multiscale nature of heterogeneous materials leads to tremendous cost for solving the thermomechanical problems by use of direct numerical methods, which also unreliable and notoriously ill-conditioned [5]. These motivate us to develop robust and efficient multiscale methods, which can not only reduce the dimensionality of coupled thermomechanical problems, but also incorporate as much microscopic important physical information as possible.

The study of multiscale methods is significant in the modeling and numerical computation of heterogeneous media, which still remain an active field in engineering practice because of its ability to fully describe intrinsic physical processes of complex systems. Great progress has been made to solve multiscale problems using various strategies, which include constrained macro simulation and generalized finite element method (GFEM) [3]. Constrained macro simulation is a micro-macro coupling interaction method, which establishes a suitable macroscopic model through solving specific microscopic problems, including homogenization method [4, 1], variational multiscale method [26], heterogeneous multiscale method [15], computational homogenization method [31], etc. The generalized finite element method was originally proposed in [3], and has been applied to solve various multiscale problems by constructing different finite element spaces. In the multiscale finite element method (MsFEM) [25], the basis functions of the finite element space are constructed by solving the local problems on each coarse block incorporated with the localized microscale physical information, and the corresponding mathematical theories are also developed for the MsFEM, such as convergence analysis and the error reduction method. Then the generalized multiscale finite element method (GMsFEM) [17, 7] is designed to obtain high accuracy multiscale basis functions by solving the local spectral problems on the snapshot spaces. Similarly, the multiscale spectral generalized finite element method (MS-GFEM) [2, 27] is another important multiscale GFEM with local approximation spaces constructed by solving local spectral problems. Moreover, the localized orthogonal decomposition (LOD) method [24, 29] stems from the ideas of the variational multiscale method [26], and the coarse space is modified with the basis functions well approximated locally. These techniques have been extended and applied the thermomechanical problems, for instance, homogenization method [20, 21, 37, 23], LOD [28], GMsFEM [36, 22] and extended MsFEM [40, 41], etc.

Inspired by previous works, this paper designed an efficient coupling formulations of GMsFEM named CGMsFEM. For the traditional GMsFEM [36] or the LOD method [28], the multiscale basis functions are separately constructed through the corresponding elliptic operators obtained by decoupling the mechanical and thermal parts of thermomechanical equations. The multiscale characteristics of the thermal expansion coefficients is not considered, which will lead to some limitations of the method. However, for CGMsFEM, the local spectral problems will be solved through an unified operator without decoupling the thermomechanical equations. The multiscale basis functions are constructed by considering the coupling effects of the displacement and temperature fields, thus the coupling information can be more accurately cap-

tured. In addition, the theoretical results of the GMSFEM method [17, 40, 41] are also generalized. The convergence analysis of the CGMSFEM is obtained, and the error estimations are derived, where the rate of decay of eigenvalues for local spectral problems is obtained, which is similar to [9]. Furthermore, several numerical examples associated with periodic, random microstructure and material coefficients are presented to confirm the theoretical analysis of CGMSFEM. When the same number of basis functions are chosen, the numerical results showed that CGMSFEM not only has better accuracy than GMSFEM in the case of weak coupling, but also has obvious advantages in the accuracy for the strong coupling situation. The novelty of the proposed approach is highlighted as follows:

- (1) The multiscale basis functions are constructed by the coupled spectral problems incorporating local multiscale physical information, which can more accurately approximate the solutions of the original thermomechanical problems with less degrees of freedom.
- (2) Two relaxation coefficients are creatively designed for the local coupling spectral problems in each coarse-grid block, the proper regularity of which is ensured by adjusting the value of relaxation coefficient. Moreover, the method can be reduced to the standard GMSFEM when the multiscale coupling correlation effect disappears, which also provides a generalized framework to design the coupling multiscale basis functions for weak or strong coupled multiphysics problems.
- (3) Through convergence analysis, it is deduced that the error of CGMSFEM is closely related to the eigenvalue decay in each local coarse block, which is consistent with GMSFEM. At the same time, it is also proved that the upper error bound is independent of the two relaxation coefficients.

The paper is organized as follows. Formulation of CGMSFEM is given in [section 2](#), including the problem statement, construction of coupling multiscale basis functions, and the corresponding finite element method. In [section 3](#), the convergence analysis of CGMSFEM is carried out. A few numerical examples are implemented to illustrate the efficiency and accuracy of the proposed CGMSFEM in [section 4](#), and the conclusions follow in [section 5](#).

2. Formulation of CGMSFEM.

2.1. Problem statement. A thermomechanical problem is considered to describe the quasi-static deformation of heterogeneous media in domain Ω , where $\Omega \subset \mathbb{R}^d$, $d = 2, 3$ is a convex bounded polygonal or polyhedral domain with Lipschitz continuous boundary $\partial\Omega$, and $T > 0$ is a given time. It is assumed that the solid phase is a linear elastic solid and the deformation is coupled with temperature field [13, 32, 11]. Then the equilibrium and heat transfer equation are written in standard as follows

$$(2.1) \quad \begin{cases} -\nabla \cdot (\boldsymbol{\sigma}(\mathbf{u}) - \beta\theta\mathbf{I}) = \mathbf{f}, & \text{in } \Omega \times (0, T], \\ \dot{\theta} - \nabla \cdot (\kappa\nabla\theta) + \beta\nabla \cdot \dot{\mathbf{u}} = g, & \text{in } \Omega \times (0, T], \end{cases}$$

where $\boldsymbol{\sigma}$ is the stress tensor, and \mathbf{I} is the d-dimensional identity matrix. $\mathbf{u}(\mathbf{x}, t) : \Omega \times (0, T] \rightarrow \mathbb{R}^d$ and $\theta(\mathbf{x}, t) : \Omega \times (0, T] \rightarrow \mathbb{R}$ denote the displacement and temperature fields, respectively. Here, the superscript dot represents partial differentiation with respect to time t and \mathbf{x} denotes the space coordinates. $\kappa(\mathbf{x})$ and $\beta(\mathbf{x})$ are the thermal conductivity and expansion coefficients with multiscale characteristic, \mathbf{f} is the body force and g is the heat source. Then the initial and boundary condition are defined

by

$$(2.2) \quad \begin{cases} \mathbf{u} = \mathbf{u}_D, & \text{on } \Gamma_D^u \times (0, T], \quad (\boldsymbol{\sigma}(u) - \beta\theta\mathbf{I}) \cdot \mathbf{n} = \boldsymbol{\sigma}_N, & \text{on } \Gamma_N^u \times (0, T], \\ \theta = \theta_D, & \text{on } \Gamma_D^\theta \times (0, T], \quad (\kappa \nabla \theta(x, t)) \cdot \mathbf{n} = q_N, & \text{on } \Gamma_N^\theta \times (0, T], \\ \theta(x, 0) = \theta_0, & \text{in } \Omega, \end{cases}$$

where the boundary of Ω is defined by surface Γ_D^u and Γ_N^u , Γ_D^θ and Γ_N^θ with $\Gamma_D^u \cap \Gamma_N^u = \emptyset$ and $\Gamma_D^\theta \cap \Gamma_N^\theta = \emptyset$. \mathbf{u}_D and θ_D are the prescribed displacement and temperature, and $\boldsymbol{\sigma}_N$ and q_N denote surface load value and heat flux, respectively. \mathbf{n} is the components of an outward vector normal to the surface Γ_N^u and Γ_N^θ . The constitutive relation of stress and strain for a general thermoelastic material is given by

$$(2.3) \quad \boldsymbol{\sigma}(\mathbf{u}) = 2\mu\boldsymbol{\epsilon}(\mathbf{u}) + \lambda\nabla \cdot \mathbf{u}\mathbf{I},$$

where $\boldsymbol{\epsilon}(\mathbf{u})$ is the strain tensor defined by

$$(2.4) \quad \boldsymbol{\epsilon}(\mathbf{u}) = \frac{1}{2}(\nabla \mathbf{u} + \nabla \mathbf{u}^T),$$

and μ and λ are the Lamé constants defined by

$$(2.5) \quad \mu = \frac{E}{2(1+\nu)}, \lambda = \frac{E\nu}{(1+\nu)(1-2\nu)},$$

where E and ν are Young's modulus and Poisson's ratio.

Here, some definitions and assumptions will firstly be stated. Let $H^1(\Omega)$ denote the classical Sobolev space equipped with the norm $\|v\|_{H^1(\Omega)}^2 = \|v\|_{L^2(\Omega)}^2 + \|\nabla v\|_{L^2(\Omega)}^2$, and $H^{-1}(\Omega)$ represents the dual space of H^1 . Then define $L_p([0, T]; V)$ for the Bochner space with the norm

$$\begin{aligned} \|v\|_{L_p([0, T]; V)} &= \left(\int_0^T \|v\|_V^p dt \right)^{\frac{1}{p}}, \quad 1 \leq p < \infty, \\ \|v\|_{L_p([0, T]; V)} &= \operatorname{ess\,inf}_{0 \leq t \leq T} \|v\|_V, \end{aligned}$$

where V is a Banach space with the norm $\|\cdot\|_V$, such as $L_2(\Omega)$ and $H^{-1}(\Omega)$. For the sake of simplicity, the time interval $[0, T]$ and the domain Ω will be omitted, for instance, $L_p(V)$ for $L_p([0, T]; V)$. The following two subspace V_u , and V_θ of H^1 are also defined as

$$V_u := \left\{ v | v \in (H^1(\Omega))^d : v = 0 \text{ on } \Gamma_D^u \right\}, \quad V_\theta := \left\{ v | v \in H^1(\Omega) : v = 0 \text{ on } \Gamma_D^\theta \right\}.$$

The following assumption is also given.

ASSUMPTION 2.1. *The material parameters $\lambda, \mu, \kappa, \beta \in L^\infty(\Omega)$ satisfied*

$$\begin{aligned} 0 \leq \lambda_{\min} &:= \operatorname{ess\,inf}_{\mathbf{x} \in \Omega} \inf_{v \in \mathbb{R}^d / \{0\}} \frac{\lambda v \cdot v}{v \cdot v} \leq \operatorname{ess\,sup}_{\mathbf{x} \in \Omega} \sup_{v \in \mathbb{R}^d / \{0\}} \frac{\lambda v \cdot v}{v \cdot v} := \lambda_{\max} \leq \infty, \\ 0 \leq \mu_{\min} &:= \operatorname{ess\,inf}_{\mathbf{x} \in \Omega} \inf_{v \in \mathbb{R}^d / \{0\}} \frac{\mu v \cdot v}{v \cdot v} \leq \operatorname{ess\,sup}_{\mathbf{x} \in \Omega} \sup_{v \in \mathbb{R}^d / \{0\}} \frac{\mu v \cdot v}{v \cdot v} := \mu_{\max} \leq \infty, \\ 0 \leq \kappa_{\min} &:= \operatorname{ess\,inf}_{\mathbf{x} \in \Omega} \inf_{v \in \mathbb{R}^d / \{0\}} \frac{\kappa v \cdot v}{v \cdot v} \leq \operatorname{ess\,sup}_{\mathbf{x} \in \Omega} \sup_{v \in \mathbb{R}^d / \{0\}} \frac{\kappa v \cdot v}{v \cdot v} := \kappa_{\max} \leq \infty, \\ 0 \leq \beta_{\min} &:= \operatorname{ess\,inf}_{\mathbf{x} \in \Omega} \inf_{v \in \mathbb{R}^d / \{0\}} \frac{\beta v \cdot v}{v \cdot v} \leq \operatorname{ess\,sup}_{\mathbf{x} \in \Omega} \sup_{v \in \mathbb{R}^d / \{0\}} \frac{\beta v \cdot v}{v \cdot v} := \beta_{\max} \leq \infty, \end{aligned}$$

where λ_{\min} , and λ_{\max} , μ_{\min} , and μ_{\max} , κ_{\min} , and κ_{\max} , β_{\min} , and β_{\max} denote upper and lower bounds of the corresponding material parameters.

Furthermore, the corresponding variational formulation of problem (2.1) is to find the weak solutions $\mathbf{u} \in V_u$ and $\theta \in V_\theta$ such that

$$(2.6) \quad \begin{cases} a(\mathbf{u}, \mathbf{v}_u) + b(\mathbf{v}_u, \theta) = \langle \mathbf{f}, \mathbf{v}_u \rangle, & \forall \mathbf{v}_u \in V_u, \\ c(\dot{\theta}, v_\theta) + d(\theta, v_\theta) + b(\dot{\mathbf{u}}, v_\theta) = \langle g, v_\theta \rangle, & \forall v_\theta \in V_\theta, \end{cases}$$

where

$$\begin{aligned} a(\mathbf{u}, \mathbf{v}_u) &= \int_{\Omega} \boldsymbol{\sigma}(\mathbf{u}) : \boldsymbol{\epsilon}(\mathbf{v}_u), & b(\mathbf{v}_u, \theta) &= \int_{\Omega} \beta \theta \nabla \cdot \mathbf{v}_u, \\ c(\dot{\theta}, v_\theta) &= \int_{\Omega} \theta v_\theta, & d(\theta, v_\theta) &= \int_{\Omega} \kappa \nabla \theta \cdot \nabla v_\theta, \end{aligned}$$

and $:$ represents the Frobenius inner product, and $\langle \cdot, \cdot \rangle$ denotes the inner product in $L^2(\Omega)$.

2.2. Construction of coupling multiscale basis functions. The procedure of the construction of CGMsFEM basis functions can be divided into two steps. Firstly, the coupling multiscale basis functions can be constructed by solving the coupling local spectral problems in coarse block, and the local computations associated with construction of local approximation spaces are independent and can be performed in parallel. Then the partition of unity functions are obtained by multiscale finite element method. Finally, the resulting global stiffness matrix can be several orders of magnitude smaller than the stiffness matrix obtained by applying FEM directly.

Suppose the domain Ω be composed of a family of meshes \mathcal{T}^H , where $H = \max_{K_i \in \mathcal{T}^H} H_{K_i}$ is the coarse mesh size and H_{K_i} is the diameter of coarse grid K_i . \mathcal{T}^H is the conforming partition of Ω , and is shape regular. \mathcal{T}^h is a conforming refinement of \mathcal{T}^H , and h is the diameter of fine grid. N denotes the number of elements in \mathcal{T}^H , and N_v denotes the number of vertices of all coarse grid. Let $\{x_i\}_{i=1}^{N_v}$ be the set of vertices in \mathcal{T}^H and $\omega_i = \bigcup \{K_j \in \mathcal{T}^H | x_i \in \overline{K_j}\}$ the neighborhood of the node x_i . Figure 2.1 depicted the fine grid, the coarse element K_i and the coarse neighborhood ω_i of the node x_i .

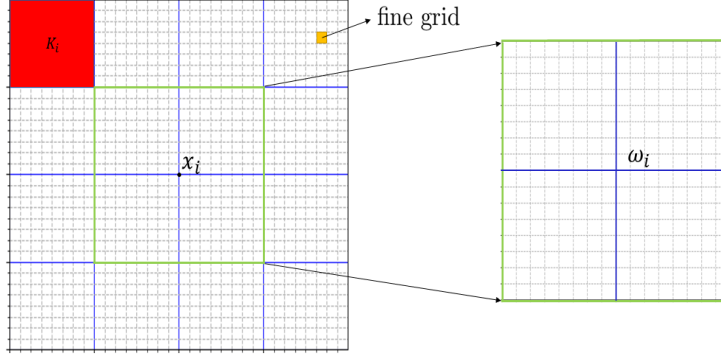


FIG. 2.1. The fine grid \mathcal{T}^h , the coarse grid \mathcal{T}^H , the coarse element K_i and neighborhood ω_i of the node x_i .

In order to construct coupling multiscale basis functions, the following coupling spectral problem in each coarse grid ω_i is given to find eigen-pairs $\{\Lambda^{\omega_i}, \psi^{\omega_i}\}$ such that

$$(2.7) \quad \begin{cases} -\nabla \cdot (\boldsymbol{\sigma}(\psi_u^{\omega_i}) - \gamma_1 \beta \psi_\theta^{\omega_i} \mathbf{I}) = \frac{1}{H^2} \Lambda^{\omega_i} (\lambda + 2\mu) \psi_u^{\omega_i}, & \text{in } \omega_i, \\ -\nabla \cdot \kappa \nabla \psi_\theta^{\omega_i} + \gamma_2 \beta \nabla \cdot \psi_u^{\omega_i} = \frac{1}{H^2} \Lambda^{\omega_i} \kappa \psi_\theta^{\omega_i}, & \text{in } \omega_i, \\ \boldsymbol{\sigma}(\psi_u^{\omega_i}) \cdot \mathbf{n} = 0, & \text{on } \partial\omega_i, \\ \kappa \nabla \psi_\theta^{\omega_i} \cdot \mathbf{n} = 0, & \text{on } \partial\omega_i, \end{cases}$$

where $\psi^{\omega_i} = (\psi_u^{\omega_i}, \psi_\theta^{\omega_i})$, and $\psi_u^{\omega_i}$ and $\psi_\theta^{\omega_i}$ are corresponding eigenfunctions for displacement and temperature fields in problem (2.7). γ_1 , and γ_2 are the relaxation coefficients, the proper regularity of which is ensured by adjusting the value of relaxation coefficient. Here, it should be emphasized that the important coupling physical characteristics are naturally incorporated into multiscale basis functions, which can obviously reduce the orders of global stiffness matrix.

Then define the classical affine finite element spaces on \mathcal{T}^h as follows

$$\begin{aligned} V_{uh} &= \left\{ \mathbf{v}_{uh} \in (L^\infty(\bar{\Omega}))^d \mid \mathbf{v}_{uh} \text{ is a polynomial of degree } \leq 1, \mathbf{v}_{uh} = 0 \text{ on } \Gamma_D^u \right\}, \\ V_{\theta h} &= \left\{ v_{\theta h} \in (L^\infty(\bar{\Omega})) \mid v_{\theta h} \text{ is a polynomial of degree } \leq 1, v_{\theta h} = 0 \text{ on } \Gamma_D^\theta \right\}. \end{aligned}$$

The corresponding variational formulation of problem (2.7) is to find the weak solutions $\psi_u^{\omega_i} \in V_{uh}$ and $\psi_\theta^{\omega_i} \in V_{\theta h}$ such that

$$(2.8) \quad \begin{cases} a^{\omega_i}(\psi_u^{\omega_i}, \mathbf{v}_{uh}) - \gamma_1 b^{\omega_i}(\mathbf{v}_{uh}, \psi_\theta^{\omega_i}) = \frac{1}{H^2} \Lambda^{\omega_i} \langle \psi_u^{\omega_i}, \mathbf{v}_{uh} \rangle_a^{\omega_i}, & \forall \mathbf{v}_{uh} \in V_{uh}, \\ d^{\omega_i}(\psi_\theta^{\omega_i}, v_{\theta h}) + \gamma_2 b^{\omega_i}(\psi_u^{\omega_i}, v_{\theta h}) = \frac{1}{H^2} \Lambda^{\omega_i} \langle \psi_\theta^{\omega_i}, v_{\theta h} \rangle_d^{\omega_i}, & \forall v_{\theta h} \in V_{\theta h}, \end{cases}$$

where

$$\begin{aligned} a^{\omega_i}(\psi_u^{\omega_i}, \mathbf{v}_{uh}) &= \int_{\omega_i} \boldsymbol{\sigma}(\psi_u^{\omega_i}) : \boldsymbol{\epsilon}(\mathbf{v}_{uh}), \quad b^{\omega_i}(\mathbf{v}_{uh}, \psi_\theta^{\omega_i}) = \int_{\omega_i} \beta \psi_\theta^{\omega_i} \nabla \cdot \mathbf{v}_{uh}, \\ d^{\omega_i}(\psi_\theta^{\omega_i}, v_{\theta h}) &= \int_{\omega_i} \kappa \nabla \psi_\theta^{\omega_i} \cdot \nabla v_{\theta h}, \\ \langle \psi_u^{\omega_i}, \mathbf{v}_{uh} \rangle_a^{\omega_i} &= \int_{\omega_i} (\lambda + 2\mu) \psi_u^{\omega_i} \cdot \mathbf{v}_{uh}, \quad \langle \psi_\theta^{\omega_i}, v_{\theta h} \rangle_d^{\omega_i} = \int_{\omega_i} \kappa \psi_\theta^{\omega_i} v_{\theta h}. \end{aligned}$$

Thus, following the standard finite element discretization, we obtain the following algebraic eigenvalue problems,

$$(2.9) \quad \mathbf{A}^{\omega_i} \psi^{\omega_i} = \frac{1}{H} \Lambda^{\omega_i} \mathbf{M}^{\omega_i} \psi^{\omega_i},$$

where

$$\mathbf{A}^{\omega_i} = \begin{bmatrix} A_1^{\omega_i} & -\gamma_1 A_2^{\omega_i} \\ \gamma_2 A_3^{\omega_i} & A_4^{\omega_i} \end{bmatrix}, \quad \mathbf{M}^{\omega_i} = \begin{bmatrix} M_1^{\omega_i} & 0 \\ 0 & M_2^{\omega_i} \end{bmatrix},$$

and

$$\begin{aligned} (A_1)_{j_1 j_1}^{\omega_i} &= a^{\omega_i}(\phi_{u,j_1}, \phi_{u,j_1}), \quad (A_2)_{j_1 j_2}^{\omega_i} = b^{\omega_i}(\phi_{u,j_1}, \phi_{\theta,j_2}), \quad A_3 = A_2^T, \\ (A_4)_{j_2 j_2}^{\omega_i} &= d^{\omega_i}(\phi_{\theta,j_2}, \phi_{\theta,j_2}), \quad (M_1)_{j_1 j_1}^{\omega_i} = \langle \phi_{u,j_1}, \phi_{u,j_1} \rangle_a^{\omega_i}, \quad (M_2)_{j_2 j_2}^{\omega_i} = \langle \phi_{\theta,j_2}, \phi_{\theta,j_2} \rangle_d^{\omega_i}, \end{aligned}$$

where $\phi_{u,j} \in V_{uh}$ and $\phi_{\theta,j} \in V_{\theta h}$, $1 \leq j_1 \leq 2N(\omega_i)$, $1 \leq j_2 \leq N(\omega_i)$, and $N(\omega_i)$ is the number of total fine grid nodes in ω_i . Moreover, the advantage of coupling multiscale basis functions from CGMsFEM compared with CGMsFEM is demonstrated in [Appendix A](#).

Then the eigenfunctions $\{\psi_l^{\omega_i}\}_{l=1}^{L_i}$ related to the smallest L_i eigenvalues are chosen as members of CGMsFEM space, which is defined by

$$(2.10) \quad V_{cgm} = \text{span} \left\{ \Phi_l^{\omega_i} \mid \Phi_l^{\omega_i} = \chi_i^T \mathbf{I}_{d+1} \psi_l^{\omega_i}, 1 \leq i \leq N_v \text{ and } 1 \leq l \leq L_i \right\},$$

where $\{\chi_i\}_{i=1}^{N_v}$ are a set of partition of unity functions associated with the open cover $\{\omega_i\}_{i=1}^{N_v}$ of domain Ω . The coupling multiscale basis function set $\{\Phi_l^{\omega_i}\}$ can be placed in the following matrix

$$(2.11) \quad \mathbf{R} = \left[\Phi_1^{\omega_1}, \Phi_2^{\omega_1} \dots, \Phi_{L_1}^{\omega_1}, \Phi_1^{\omega_2}, \Phi_2^{\omega_2} \dots, \Phi_{L_2}^{\omega_2}, \dots, \Phi_1^{\omega_{N_v}}, \Phi_2^{\omega_{N_v}} \dots, \Phi_{L_{N_v}}^{\omega_{N_v}} \right],$$

Here, it should be noted that the matrix \mathbf{R} only needs to be constructed once, and it can be repeatedly used for computation.

2.3. Algorithm procedure of CGMsFEM. In the paper, the backward Euler scheme is used for temporal discretization. Let $\mathbf{w}^n = (\mathbf{u}_h^n, \theta_h^n)$ be the solutions at the n -th time level $t_n = \sum_{m=1}^n \tau_m$, $n \in \{0, 1, \dots, N_T\}$, where τ_m is the time step. Then we have the following weak formulation for the equation [\(2.6\)](#),

$$(2.12) \quad \begin{cases} a(\mathbf{u}_h^n, \mathbf{v}_{uh}) + b(\mathbf{v}_{uh}, \theta_h^n) = \langle \mathbf{f}^n, \mathbf{v}_{uh} \rangle, & \forall \mathbf{v}_{uh} \in V_{uh}, \\ c\left(\frac{\theta_h^n - \theta_h^{n-1}}{\tau_n}, v_{\theta h}\right) + d(\theta_h^n, v_{\theta h}) + b\left(\frac{\mathbf{u}_h^n - \mathbf{u}_h^{n-1}}{\tau_n}, v_{\theta h}\right) = \langle g^n, v_{\theta h} \rangle, & \forall v_{\theta h} \in V_{\theta h}, \end{cases}$$

Thus, following the standard finite element discretization, Eqs. (2.12) can be rewritten as follows

$$(2.13) \quad \mathbf{A}^n \mathbf{w}^n = \mathbf{B} \mathbf{w}^{n-1} + \mathbf{F}^n,$$

where

$$\mathbf{A}^n = \begin{bmatrix} A_1 & -A_2 \\ A_3 & M' + \tau_n A_4 \end{bmatrix}, \mathbf{B} = \begin{bmatrix} 0 & 0 \\ A_3 & M' \end{bmatrix}, \mathbf{F}^n = \begin{bmatrix} F^n \\ \tau G^n \end{bmatrix},$$

and

$$\begin{aligned} (A_1)_{j_1 j_1} &= a(\phi_{u,j_1}, \phi_{u,j_1}), \quad (A_2)_{j_1 j_2} = b(\phi_{u,j_1}, \phi_{\theta,j_2}), \quad A_3 = A_2^T, \\ (A_4)_{j_2 j_2} &= d(\phi_{\theta,j_2}, \phi_{\theta,j_2}), \quad (M')_{j_2 j_2} = c(\phi_{\theta,j_2}, \phi_{\theta,j_2}), \\ (F^n)_{j_1} &= (\mathbf{f}^n, \phi_{u,j_1}), \quad (G^n)_{j_2} = (g^n, \phi_{\theta,j_2}). \end{aligned}$$

Define

$$\mathbf{A}_c^n = \mathbf{R}^T \mathbf{A}^n \mathbf{R}, \quad \mathbf{B}^c = \mathbf{R}^T \mathbf{B} \mathbf{R}, \quad \mathbf{w}_c^n = (\mathbf{R}^T \mathbf{R})^{-1} \mathbf{R}^T \mathbf{w}^n, \quad \mathbf{F}_c^n = (\mathbf{R}^T \mathbf{R})^{-1} \mathbf{R}^T \mathbf{F}^n,$$

and combining with Eq. (2.13), the following algebraic system can be given,

$$(2.14) \quad \mathbf{A}_c^n \mathbf{w}_c^n = \mathbf{B}^c \mathbf{w}_c^{n-1} + \mathbf{F}_c^n,$$

Then the solution \mathbf{w}_c^n can be calculated by iteration, and the solutions in fine grid can be obtained by use of the coupling multiscale basis functions,

$$(2.15) \quad \mathbf{w}^n = \mathbf{R} \mathbf{w}_c^n.$$

Here, the key difference between CGMsFEM and GMSFEM is the construction of more accurate coupling multiscale basis functions. The matrix \mathbf{R} can be computed offline, and they can be reused in all time steps. Thus, a much smaller system is solved with CGMsFEM, which can significantly improve the computational efficiency.

3. Convergence analysis of CGMsFEM.

3.1. Interpolation error. Before proving the convergence and error estimates for CGMsFEM, some definitions and Lemmas are firstly given. Let $\mathbf{w} = (\mathbf{u}, \theta)$, $\mathbf{v} = (\mathbf{v}_u, v_\theta) \in V_u \times V_\theta$, and define the bilinear functionals

$$(3.1) \quad \begin{aligned} \mathcal{A}(\mathbf{w}, \mathbf{v}) &= a(\mathbf{u}, \mathbf{v}_u) - \gamma_1 b(\mathbf{v}_u, \theta) + \gamma_2 b(\mathbf{u}, v_\theta) + d(\theta, v_\theta), \\ \mathcal{M}(\mathbf{w}, \mathbf{v}) &= \int_{\Omega} (\lambda + 2\mu) \mathbf{u} \cdot \mathbf{v}_u + \kappa \theta v_\theta. \end{aligned}$$

Then the global eigenvalue problem can be written as

$$(3.2) \quad \mathcal{A}(\psi, \mathbf{v}) = \Lambda \mathcal{M}(\psi, \mathbf{v}), \quad \forall \mathbf{v} \in V_u(\Omega) \times V_\theta(\Omega).$$

The $b(\cdot, \cdot)$ is continuous in $V_u(\Omega) \times L^2(\Omega)$, and it can be assumed that there exists a constant C_0 such that for all $\mathbf{u} \in V_u(\Omega)$, $\theta \in L_2(\Omega)$, we have

$$(3.3) \quad b^K(\mathbf{u}, \theta) \leq C_0 \|\mathbf{u}\|_{a,K} \|\theta\|_{L_d,K}, \quad \forall K \in \mathcal{T}_H,$$

where

$$\|\theta\|_{L_d,K}^2 = \int_K \kappa \theta^2.$$

Also define

$$\|\mathbf{u}\|_{L_{a,K}}^2 = \int_K (\lambda + 2\mu) \mathbf{u} \cdot \mathbf{u}.$$

Then for all $\mathbf{u} \in V_u(\Omega), \theta \in V_\theta(\Omega)$, the energy norms can be defined as follows

$$(3.4) \quad \|\mathbf{u}\|_{a,\tilde{\Omega}}^2 = a^{\tilde{\Omega}}(\mathbf{u}, \mathbf{u}), \quad \|\theta\|_{d,\tilde{\Omega}}^2 = d^{\tilde{\Omega}}(\theta, \theta), \quad \tilde{\Omega} \subset \Omega.$$

Hereafter $\tilde{\Omega}$ can be K or ω_i . Meanwhile, the local bilinear functionals can be defined as follows

$$(3.5) \quad \begin{aligned} \mathcal{A}^{\tilde{\Omega}}(\mathbf{w}, \mathbf{v}) &= a^{\tilde{\Omega}}(\mathbf{u}, \mathbf{v}_u) - \gamma_1 b^{\tilde{\Omega}}(\mathbf{v}_u, \theta) + \gamma_2 b^{\tilde{\Omega}}(\mathbf{u}, v_\theta) + d^{\tilde{\Omega}}(\theta, v_\theta), \\ \mathcal{M}^{\tilde{\Omega}}(\mathbf{w}, \mathbf{v}) &= \int_{\tilde{\Omega}} (\lambda + 2\mu) \mathbf{u} \cdot \mathbf{v}_u + \kappa \theta v_\theta. \end{aligned}$$

Then the local eigenvalue problem (2.7) can be written as

$$(3.6) \quad \mathcal{A}^{\omega_i}(\psi^{\omega_i}, \mathbf{v}) = \frac{1}{H^2} \Lambda^{\omega_i} \mathcal{M}^{\omega_i}(\psi^{\omega_i}, \mathbf{v}), \quad \forall \mathbf{v} \in V_u(\omega_i) \times V_\theta(\omega_i).$$

The obtained eigenvalues can be arranged in ascending order

$$(3.7) \quad \Lambda_1^{\omega_i} \leq \Lambda_2^{\omega_i} \leq \dots \leq \Lambda_L^{\omega_i} \leq \dots$$

Assume that the eigenvalues are all real numbers and are bigger than 0, and define

$$(3.8) \quad \tilde{V}(\omega_i) = \left\{ \mathbf{v} \in V_u(\omega_i) \times V_\theta(\omega_i) : \int_{\omega_i} \mathbf{v} = 0 \right\},$$

we have

$$(3.9) \quad \mathbf{v} = \sum_{l=1}^{\infty} \mathcal{M}^{\omega_i}(\mathbf{v}, \psi_l^{\omega_i}) \psi_l^{\omega_i}, \quad \forall \mathbf{v} \in \tilde{V}(\omega_i),$$

where $\{\psi^{\omega_i}\}$ are a set of complete orthogonal basis functions in $M^{\omega_i}(\cdot, \cdot)$ with the inner product defined in $\tilde{V}(\omega_i)$. It is easily obtained as follows

$$(3.10) \quad \mathcal{A}^{\omega_i}(\mathbf{v}, \mathbf{v}) = \frac{1}{H^2} \sum_{l=1}^{\infty} \mathcal{M}^{\omega_i}(\mathbf{v}, \psi_l^{\omega_i})^2 \Lambda_l^{\omega_i}, \quad \mathcal{M}^{\omega_i}(\mathbf{v}, \mathbf{v}) = \sum_{l=1}^{\infty} \mathcal{M}^{\omega_i}(\mathbf{v}, \psi_l^{\omega_i})^2.$$

Define the semi-norm by

$$(3.11) \quad \|\mathbf{v}\|_{s,\omega_i}^2 = \sum_{l=1}^{\infty} \left(\frac{\Lambda_l^{\omega_i}}{H^2} \right)^s \mathcal{M}^{\omega_i}(\mathbf{v}, \psi_l^{\omega_i})^2,$$

and it follows that

$$(3.12) \quad \|\mathbf{v}\|_{0,\omega_i}^2 = \mathcal{M}^{\omega_i}(\mathbf{v}, \mathbf{v}), \quad \|\mathbf{v}\|_{1,\omega_i}^2 = \mathcal{A}^{\omega_i}(\mathbf{v}, \mathbf{v}).$$

Following the above definitions, we give

LEMMA 3.1. Assume that $\mathbf{w} \in V_u(\omega_i) \times V_\theta(\omega_i)$, $\partial_n \mathbf{w} = 0$ in $\partial\omega_i$, and $\|\mathbf{w}\|_{s,\omega_i} \leq \infty$. For $0 \leq t \leq s$, there holds

$$(3.13) \quad \|\mathbf{w} - \mathcal{I}_{L_i}^{\omega_i} \mathbf{w}\|_{t,\omega_i}^2 \leq \left(\frac{\Lambda_{L_i+1}^{\omega_i}}{H^2}\right)^{t-s} \|\mathbf{w}\|_{s,\omega_i}^2,$$

where $\mathcal{I}_{L_i}^{\omega_i}$ is the local interpolation operator defined by

$$(3.14) \quad \mathcal{I}_{L_i}^{\omega_i} \mathbf{w} = \sum_{l=1}^{L_i} \mathcal{M}^{\omega_i}(\mathbf{w}, \psi_l^{\omega_i}) \psi_l^{\omega_i}.$$

PROOF. By definition (3.14), it can be obtained that

$$\begin{aligned} \|\mathbf{w} - \mathcal{I}_{L_i}^{\omega_i} \mathbf{w}\|_{t,\omega_i}^2 &= \sum_{l=L_i+1}^{\infty} \left(\frac{\Lambda_l^{\omega_i}}{H^2}\right)^t \mathcal{M}^{\omega_i}(\mathbf{w}, \psi_l^{\omega_i})^2 \\ &= \sum_{l=L_i+1}^{\infty} \left(\frac{\Lambda_l^{\omega_i}}{H^2}\right)^{t-s} \left(\frac{\Lambda_l^{\omega_i}}{H^2}\right)^s \mathcal{M}^{\omega_i}(\mathbf{w}, \psi_l^{\omega_i})^2 \\ &\leq \left(\frac{\Lambda_{L_i+1}^{\omega_i}}{H^2}\right)^{t-s} \sum_{l=L_i+1}^{\infty} \left(\frac{\Lambda_l^{\omega_i}}{H^2}\right)^s \mathcal{M}^{\omega_i}(\mathbf{w}, \psi_l^{\omega_i})^2 \\ &\leq \left(\frac{\Lambda_{L_i+1}^{\omega_i}}{H^2}\right)^{t-s} \|\mathbf{w} - \mathcal{I}_{L_i}^{\omega_i} \mathbf{w}\|_{s,\omega_i}^2 \\ &\leq \left(\frac{\Lambda_{L_i+1}^{\omega_i}}{H^2}\right)^{t-s} \|\mathbf{w}\|_{s,\omega_i}^2. \end{aligned}$$

Then the following corollary can be given by this lemma with $t = 0, 1$.

COROLLARY 3.1. For all $\mathbf{w} \in V_u(\omega_i) \times V_\theta(\omega_i)$,

$$(3.15) \quad \begin{aligned} \mathcal{M}^{\omega_i}(\mathbf{w} - \mathcal{I}_{L_i}^{\omega_i} \mathbf{w}, \mathbf{w} - \mathcal{I}_{L_i}^{\omega_i} \mathbf{w}) &\leq \frac{H^{2s}}{(\Lambda_{L_i+1}^{\omega_i})^s} \|\mathbf{w}\|_{s,\omega_i}^2, \\ \mathcal{A}^{\omega_i}(\mathbf{w} - \mathcal{I}_{L_i}^{\omega_i} \mathbf{w}, \mathbf{w} - \mathcal{I}_{L_i}^{\omega_i} \mathbf{w}) &\leq \frac{H^{2s-2}}{(\Lambda_{L_i+1}^{\omega_i})^{s-1}} \|\mathbf{w}\|_{s,\omega_i}^2. \end{aligned}$$

For interpolation operator $\mathcal{I}: V_u \times V_\theta \rightarrow V_u \times V_\theta$ and all $\mathbf{w} = (\mathbf{u}, \theta) \in V_u \times V_\theta$, we define $(\mathcal{I}\mathbf{w})_u$ and $(\mathcal{I}\mathbf{w})_\theta$, s.t. $\mathcal{I}\mathbf{w} = ((\mathcal{I}\mathbf{w})_u, (\mathcal{I}\mathbf{w})_\theta)$.

LEMMA 3.2. For all $\mathbf{w} = (\mathbf{u}, \theta) \in V_u(\Omega) \times V_\theta(\Omega)$, there holds

$$(3.16) \quad \begin{aligned} \int_K (\lambda + 2\mu) (\mathbf{u} - (\mathcal{I}_{ms}\mathbf{w})_u) \cdot (\mathbf{u} - (\mathcal{I}_{ms}\mathbf{w})_u) + \kappa (\theta - (\mathcal{I}_{ms}\mathbf{w})_\theta)^2 \\ \leq N_K \frac{H^4}{\Lambda_{K,L+1}} \sum_{y_i \in K} \|\mathbf{w}\|_{2,\omega_i}^2, \end{aligned}$$

where $N_K = \text{card}\{y_i : y_i \in K\}$ and $\Lambda_{K,L+1} = \min_{y_i \in K} \Lambda_{L_i+1}^{\omega_i}$. $\mathcal{I}_{ms}: V_u(\Omega) \times V_\theta(\Omega) \rightarrow V_{cgm}$ is the global interpolation operator, which is defined by

$$(3.17) \quad \mathcal{I}_{ms}\mathbf{w} = \sum_{i=1}^{N_v} \sum_{l=1}^{L_i} \mathcal{M}^{\omega_i}(\mathbf{w}, \psi_l^{\omega_i}) \Phi_l^{\omega_i}.$$

PROOF. Based on the definition of \mathcal{I}_{ms} , we have

$$\begin{aligned}
 \mathbf{w} - \mathcal{I}_{ms}\mathbf{w} &= \mathbf{w} - \sum_{i=1}^{N_v} \sum_{l=1}^{L_i} \mathcal{M}^{\omega_i}(\mathbf{w}, \psi_l^{\omega_i}) \chi_i^T(x) I_{d+1} \psi_l^{\omega_i} \\
 (3.18) \quad &= \mathbf{w} - \sum_{i=1}^{N_v} \chi_i^T I_{d+1} \mathcal{I}_{L_i}^{\omega_i} \mathbf{w} \\
 &= \sum_{i=1}^{N_v} \chi_i^T(x) I_{d+1} (\mathbf{w} - \mathcal{I}_{L_i}^{\omega_i} \mathbf{w}).
 \end{aligned}$$

Combining with Eq. (3.18), the left part of Eq. (3.16) gives

$$\begin{aligned}
 (3.19) \quad & \int_K (\lambda + 2\mu) \left(\sum_{y_i \in K} \chi_{i,u}^T I_d (\mathbf{u} - (\mathcal{I}_{L_i}^{\omega_i} \mathbf{w})_u) \right) \cdot \left(\sum_{y_i \in K} \chi_{i,u}^T I_d (\mathbf{u} - (\mathcal{I}_{L_i}^{\omega_i} \mathbf{w})_u) \right) \\
 & + \kappa \left(\sum_{y_i \in K} \chi_{i,\theta} \left(\theta - (\mathcal{I}_{L_i}^{\omega_i} \mathbf{w})_\theta \right) \right)^2 \\
 & \leq N_K \sum_{y_i \in K} \int_K (\lambda + 2\mu) \left(\chi_{i,u}^T I_d (\mathbf{u} - (\mathcal{I}_{L_i}^{\omega_i} \mathbf{w})_u) \right) \cdot \left(\chi_{i,u}^T I_d (\mathbf{u} - (\mathcal{I}_{L_i}^{\omega_i} \mathbf{w})_u) \right) \\
 & + \kappa \left(\chi_{i,\theta} \left(\theta - (\mathcal{I}_{L_i}^{\omega_i} \mathbf{w})_\theta \right) \right)^2 \\
 & \leq N_K \sum_{y_i \in K} \int_{\omega_i} (\lambda + 2\mu) \left(\mathbf{u} - (\mathcal{I}_{L_i}^{\omega_i} \mathbf{w})_u \right) \cdot \left(\mathbf{u} - (\mathcal{I}_{L_i}^{\omega_i} \mathbf{w})_u \right) + \kappa \left(\theta - (\mathcal{I}_{L_i}^{\omega_i} \mathbf{w})_\theta \right)^2 \\
 & = N_K \sum_{y_i \in K} \mathcal{M}^{\omega_i}(\mathbf{w} - \mathcal{I}_{L_i}^{\omega_i} \mathbf{w}, \mathbf{w} - \mathcal{I}_{L_i}^{\omega_i} \mathbf{w}) \\
 & \leq N_K \sum_{y_i \in K} \frac{H^4}{(\Lambda_{L_i+1}^{\omega_i})^2} \|\mathbf{w}\|_{2,\omega_i}^2 \\
 & \leq N_K \frac{H^4}{(\Lambda_{K,L+1})^2} \sum_{y_i \in K} \|\mathbf{w}\|_{2,\omega_i}^2.
 \end{aligned}$$

LEMMA 3.3. For all $\mathbf{w} = (\mathbf{u}, \theta) \in V_u(\Omega) \times V_\theta(\Omega)$ and the definition of \mathcal{I}_{ms} , the local interpolation error estimate can be given as

$$\begin{aligned}
 (3.20) \quad & \|\mathbf{u} - (\mathcal{I}_{ms}\mathbf{w})_u\|_{a,K} + \|\theta - (\mathcal{I}_{ms}\mathbf{w})_\theta\|_{d,K} \leq 2N_K \sum_{y_i \in K} \left(C_2 \mathcal{A}^K(\mathbf{w} - \mathcal{I}_{ms}\mathbf{w}, \mathbf{w} - \mathcal{I}_{ms}\mathbf{w}) \right. \\
 & \quad \left. + \left(\frac{2C_1^2}{H^2} + C_3 \right) \left(\|\mathbf{u} - (\mathcal{I}_{ms}\mathbf{w})_u\|_{L_{a,K}} + \|\theta - (\mathcal{I}_{ms}\mathbf{w})_\theta\|_{L_{d,K}} \right) \right).
 \end{aligned}$$

where $C_2 = \frac{2}{2 - |\gamma_1 - \gamma_2|C_0}$, $C_3 = \frac{|\gamma_1 - \gamma_2|C_0}{2 - |\gamma_1 - \gamma_2|C_0}$.

PROOF. Firstly, the local energy error of the interpolation operator \mathcal{I}_{ms} can be

given as

$$\begin{aligned}
 & a^K(\mathbf{u} - (\mathcal{I}_{ms}\mathbf{w})_u, \mathbf{u} - (\mathcal{I}_{ms}\mathbf{w})_u) + d^K(\theta - (\mathcal{I}_{ms}\mathbf{w})_\theta, \theta - (\mathcal{I}_{ms}\mathbf{w})_\theta) \\
 &= \int_K 2\mu \epsilon(\mathbf{u} - (\mathcal{I}_{ms}\mathbf{w})_u) : \epsilon(\mathbf{u} - (\mathcal{I}_{ms}\mathbf{w})_u) + \int_K \lambda \nabla \cdot (\mathbf{u} - (\mathcal{I}_{ms}\mathbf{w})_u) \\
 & \quad \nabla \cdot (\mathbf{u} - (\mathcal{I}_{ms}\mathbf{w})_u) + \int_K \kappa \nabla(\theta - (\mathcal{I}_{ms}\mathbf{w})_\theta) \cdot \nabla(\theta - (\mathcal{I}_{ms}\mathbf{w})_\theta) \\
 & \equiv I_1 + I_2 + I_3.
 \end{aligned} \tag{3.21}$$

Define $E(u) : \mathbb{R}^d \rightarrow \mathbb{R}^{d \times d}$ with $E(u)|_{ij} = \frac{1}{2}(u_i + u_j)$ for all $u \in V_u(\Omega)$, it follows that

$$\max |\nabla \chi_i| \leq \frac{C_1}{H}, \quad \forall i \leq N_v. \tag{3.22}$$

and \circ is Hadamard product, for any $K \in \mathcal{T}_H$, we have

$$\begin{aligned}
 \epsilon(\mathbf{u} - (\mathcal{I}_{ms}\mathbf{w})_u) &= \epsilon \left(\sum_{y_i \in K} \chi_{i,u}^T I_d \left(\mathbf{u} - (\mathcal{I}_{L_i}^{\omega_i} \mathbf{w})_u \right) \right) \\
 &= \sum_{y_i \in K} \left(E(\chi_{i,u}) \circ \epsilon \left(\mathbf{u} - (\mathcal{I}_{L_i}^{\omega_i} \mathbf{w})_u \right) + E \left(\mathbf{u} - (\mathcal{I}_{L_i}^{\omega_i} \mathbf{w})_u \right) \circ \epsilon(\chi_{i,u}) \right).
 \end{aligned} \tag{3.23}$$

Then I_1 can be estimated as follows

$$\begin{aligned}
 I_1 &\leq 2N_K \sum_{y_i \in K} \left(\int_K 2\mu E(\chi_{i,u}) \circ \epsilon \left(\mathbf{u} - (\mathcal{I}_{L_i}^{\omega_i} \mathbf{w})_u \right) : E(\chi_{i,u}) \circ \epsilon \left(\mathbf{u} - (\mathcal{I}_{L_i}^{\omega_i} \mathbf{w})_u \right) \right. \\
 & \quad \left. + \int_K 2\mu E \left(\mathbf{u} - (\mathcal{I}_{L_i}^{\omega_i} \mathbf{w})_u \right) \circ \epsilon(\chi_{i,u}) : E \left(\mathbf{u} - (\mathcal{I}_{L_i}^{\omega_i} \mathbf{w})_u \right) \circ \epsilon(\chi_{i,u}) \right) \\
 &\leq 2N_K \sum_{y_i \in K} \left(\int_K 2\mu \epsilon \left(\mathbf{u} - (\mathcal{I}_{L_i}^{\omega_i} \mathbf{w})_u \right) : \epsilon \left(\mathbf{u} - (\mathcal{I}_{L_i}^{\omega_i} \mathbf{w})_u \right) \right. \\
 & \quad \left. + \frac{C_1^2}{H^2} \int_K 2\mu E \left(\mathbf{u} - (\mathcal{I}_{L_i}^{\omega_i} \mathbf{w})_u \right) : E \left(\mathbf{u} - (\mathcal{I}_{L_i}^{\omega_i} \mathbf{w})_u \right) \right), \\
 &\leq 2N_K \sum_{y_i \in K} \left(\int_K 2\mu \epsilon \left(\mathbf{u} - (\mathcal{I}_{L_i}^{\omega_i} \mathbf{w})_u \right) : \epsilon \left(\mathbf{u} - (\mathcal{I}_{L_i}^{\omega_i} \mathbf{w})_u \right) \right. \\
 & \quad \left. + \frac{C_1^2}{H^2} 2 \int_K 2\mu \left(\mathbf{u} - (\mathcal{I}_{L_i}^{\omega_i} \mathbf{w})_u \right) \cdot \left(\mathbf{u} - (\mathcal{I}_{L_i}^{\omega_i} \mathbf{w})_u \right) \right).
 \end{aligned} \tag{3.24}$$

Next, I_2 can be estimated for any $K \in \mathcal{T}_H$ as follows

$$\begin{aligned}
 \nabla \cdot (\mathbf{u} - (\mathcal{I}_{ms}\mathbf{w})_u) &= \sum_{y_i \in K} \nabla \cdot \left(\chi_{i,u}^T I_d \left(\mathbf{u} - (\mathcal{I}_{L_i}^{\omega_i} \mathbf{w})_u \right) \right) \\
 &= \sum_{y_i \in K} \left(\text{diag}(\chi_{i,u}) : \nabla \left(\mathbf{u} - (\mathcal{I}_{L_i}^{\omega_i} \mathbf{w})_u \right) + \text{diag} \left(\mathbf{u} - (\mathcal{I}_{L_i}^{\omega_i} \mathbf{w})_u \right) : \nabla(\chi_{i,u}) \right),
 \end{aligned} \tag{3.25}$$

where $\text{diag}(\cdot)$ represents the main diagonal elements of square matrix. Thus,

$$\begin{aligned}
 I_2 &\leq 2N_K \sum_{y_i \in K} \left(\int_K \lambda \left(\text{diag}(\chi_{i,u}) : \nabla \left(\mathbf{u} - (\mathcal{I}_{L_i}^{\omega_i} \mathbf{w})_u \right) \right)^2 \right. \\
 &\quad \left. + \left(\text{diag}(\mathbf{u} - (\mathcal{I}_{L_i}^{\omega_i} \mathbf{w})_u) : \nabla (\chi_{i,u}) \right)^2 \right) \\
 (3.26) \quad &\leq 2N_K \sum_{y_i \in K} \left(\int_K \lambda \left(\nabla \cdot \left(\mathbf{u} - (\mathcal{I}_{L_i}^{\omega_i} \mathbf{w})_u \right) \right)^2 \right. \\
 &\quad \left. + \frac{2C_1^2}{H^2} \left(\mathbf{u} - (\mathcal{I}_{L_i}^{\omega_i} \mathbf{w})_u \right) \cdot \left(\mathbf{u} - (\mathcal{I}_{L_i}^{\omega_i} \mathbf{w})_u \right) \right).
 \end{aligned}$$

Combining Eq. (3.24) with Eq. (3.26), it follows that

$$\begin{aligned}
 I_1 + I_2 &\leq 2N_K \sum_{y_i \in K} \left(\left\| \mathbf{u} - (\mathcal{I}_{L_i}^{\omega_i} \mathbf{w})_u \right\|_{a,K}^2 \right. \\
 (3.27) \quad &\quad \left. + \frac{2C_1^2}{H^2} \int_K (2\mu + \lambda) \left(\mathbf{u} - (\mathcal{I}_{L_i}^{\omega_i} \mathbf{w})_u \right) \cdot \left(\mathbf{u} - (\mathcal{I}_{L_i}^{\omega_i} \mathbf{w})_u \right) \right).
 \end{aligned}$$

Next, I_3 can be estimated for any $K \in \mathcal{T}_H$, and define

$$\begin{aligned}
 \nabla (\theta - (\mathcal{I}_{ms} \mathbf{w})_\theta) &= \sum_{y_i \in K} \nabla \left(\chi_{i,\theta} \left(\theta - (\mathcal{I}_{L_i}^{\omega_i} \mathbf{w})_\theta \right) \right) \\
 (3.28) \quad &= \sum_{y_i \in K} \left(\chi_{i,\theta} \nabla \left(\theta - (\mathcal{I}_{L_i}^{\omega_i} \mathbf{w})_\theta \right) + \left(\theta - (\mathcal{I}_{L_i}^{\omega_i} \mathbf{w})_\theta \right) \nabla \chi_{i,\theta} \right).
 \end{aligned}$$

Substituting it into I_3 , we obtain

$$\begin{aligned}
 I_3 &\leq 2N_K \sum_{y_i \in K} \left(\int_K \kappa \left(\chi_{i,\theta} \nabla \left(\theta - (\mathcal{I}_{L_i}^{\omega_i} \mathbf{w})_\theta \right) \right) \cdot \left(\chi_{i,\theta} \nabla \left(\theta - (\mathcal{I}_{L_i}^{\omega_i} \mathbf{w})_\theta \right) \right) \right. \\
 &\quad \left. + \int_K \kappa \left(\left(\theta - (\mathcal{I}_{L_i}^{\omega_i} \mathbf{w})_\theta \right) \nabla \chi_{i,\theta} \right) \cdot \left(\left(\theta - (\mathcal{I}_{L_i}^{\omega_i} \mathbf{w})_\theta \right) \nabla \chi_{i,\theta} \right) \right) \\
 (3.29) \quad &\leq 2N_K \sum_{y_i \in K} \left(\int_K \kappa \nabla \left(\theta - (\mathcal{I}_{L_i}^{\omega_i} \mathbf{w})_\theta \right) \cdot \nabla \left(\theta - (\mathcal{I}_{L_i}^{\omega_i} \mathbf{w})_\theta \right) \right. \\
 &\quad \left. + \frac{2C_1^2}{H^2} \int_K \kappa \left(\theta - (\mathcal{I}_{L_i}^{\omega_i} \mathbf{w})_\theta \right)^2 \right).
 \end{aligned}$$

Combining Eq. (3.27) and Eq. (3.29), it follows that

$$\begin{aligned}
 I_1 + I_2 + I_3 &\leq 2N_K \sum_{y_i \in K} \left(\left\| \mathbf{u} - (\mathcal{I}_{L_i}^{\omega_i} \mathbf{w})_u \right\|_{a,K}^2 + \left\| \theta - (\mathcal{I}_{L_i}^{\omega_i} \mathbf{w})_\theta \right\|_{d,K}^2 + \right. \\
 (3.30) \quad &\quad \left. \frac{2C_1^2}{H^2} \left(\left\| \mathbf{u} - (\mathcal{I}_{L_i}^{\omega_i} \mathbf{w})_u \right\|_{L_{a,K}} + \left\| \theta - (\mathcal{I}_{L_i}^{\omega_i} \mathbf{w})_\theta \right\|_{L_{d,K}} \right) \right).
 \end{aligned}$$

Moreover, define $J = \left\| \mathbf{u} - (\mathcal{I}_{L_i}^{\omega_i} \mathbf{w})_u \right\|_{a,K}^2 + \left\| \theta - (\mathcal{I}_{L_i}^{\omega_i} \mathbf{w})_\theta \right\|_{d,K}^2$, then

$$\begin{aligned}
 (3.31) \quad J &= \mathcal{A}^K (\mathbf{w} - \mathcal{I}_{L_i}^{\omega_i} \mathbf{w}, \mathbf{w} - \mathcal{I}_{L_i}^{\omega_i} \mathbf{w}) + (\gamma_1 - \gamma_2) b^K \left(\mathbf{u} - (\mathcal{I}_{L_i}^{\omega_i} \mathbf{w})_u, \theta - (\mathcal{I}_{L_i}^{\omega_i} \mathbf{w})_\theta \right) \\
 &\leq \mathcal{A}^K (\mathbf{w} - \mathcal{I}_{L_i}^{\omega_i} \mathbf{w}, \mathbf{w} - \mathcal{I}_{L_i}^{\omega_i} \mathbf{w}) + |\gamma_1 - \gamma_2| C_0 \left\| \mathbf{u} - (\mathcal{I}_{L_i}^{\omega_i} \mathbf{w})_u \right\|_{a,K} \left\| \theta - (\mathcal{I}_{L_i}^{\omega_i} \mathbf{w})_\theta \right\|_{L_d,K} \\
 &\leq \mathcal{A}^K (\mathbf{w} - \mathcal{I}_{L_i}^{\omega_i} \mathbf{w}, \mathbf{w} - \mathcal{I}_{L_i}^{\omega_i} \mathbf{w}) + \frac{|\gamma_1 - \gamma_2| C_0}{2} \\
 &\quad \left(\left\| \mathbf{u} - (\mathcal{I}_{L_i}^{\omega_i} \mathbf{w})_u \right\|_{a,K}^2 + \left\| \theta - (\mathcal{I}_{L_i}^{\omega_i} \mathbf{w})_\theta \right\|_{L_d,K}^2 \right) \\
 &\leq \mathcal{A}^K (\mathbf{w} - \mathcal{I}_{L_i}^{\omega_i} \mathbf{w}, \mathbf{w} - \mathcal{I}_{L_i}^{\omega_i} \mathbf{w}) + \frac{|\gamma_1 - \gamma_2| C_0}{2} \left(J + \left\| \theta - (\mathcal{I}_{L_i}^{\omega_i} \mathbf{w})_\theta \right\|_{L_d,K}^2 \right).
 \end{aligned}$$

Then let $C_2 = \frac{2}{2 - |\gamma_1 - \gamma_2| C_0}$, $C_3 = \frac{|\gamma_1 - \gamma_2| C_0}{2 - |\gamma_1 - \gamma_2| C_0}$, and assume $\frac{|\gamma_1 - \gamma_2| C_0}{2} < 1$, it follows that

$$(3.32) \quad J \leq C_2 \mathcal{A}^K (\mathbf{w} - \mathcal{I}_{L_i}^{\omega_i} \mathbf{w}, \mathbf{w} - \mathcal{I}_{L_i}^{\omega_i} \mathbf{w}) + C_3 \left\| \theta - (\mathcal{I}_{L_i}^{\omega_i} \mathbf{w})_\theta \right\|_{L_d,K}^2.$$

Finally, combining (3.21), (3.30) with (3.32), this proof is complete.

Lemma 3.3 directly leads to the following estimation of global interpolation error.

THEOREM 3.1. For all $\mathbf{w} \in V_u(\Omega) \times V_\theta(\Omega)$ and definition of \mathcal{I}_{ms} , the global interpolation error can be given as

$$\begin{aligned}
 (3.33) \quad &\left\| \mathbf{u} - (\mathcal{I}_{ms} \mathbf{w})_u \right\|_{a,\Omega}^2 + \left\| \theta - (\mathcal{I}_{ms} \mathbf{w})_\theta \right\|_{d,\Omega}^2 \\
 &\leq 2N_{max} \left(C_2 \frac{H^2}{\Lambda_{L+1}} + (2C_1^2 H^2 + C_3 H^4) \frac{1}{(\Lambda_{L+1})^2} \right) \sum_{\omega_i} \|\mathbf{w}\|_{2,\omega_i}^2,
 \end{aligned}$$

where $\Lambda_{L+1} = \min_{\omega_i} \Lambda_{L_i+1}^{\omega_i}$ and $N_{max} = \max_K N_K$.

PROOF. From Eq.(3.20), the following estimations can be given as

$$\begin{aligned}
 (3.34) \quad &\sum_{K \in \mathcal{T}^H} \sum_{y_i \in K} \mathcal{A}^K (\mathbf{w} - \mathcal{I}_{L_i}^{\omega_i} \mathbf{w}, \mathbf{w} - \mathcal{I}_{L_i}^{\omega_i} \mathbf{w}) = \sum_{\omega_i} \mathcal{A}^{\omega_i} (\mathbf{w} - \mathcal{I}_{L_i}^{\omega_i} \mathbf{w}, \mathbf{w} - \mathcal{I}_{L_i}^{\omega_i} \mathbf{w}) \\
 &\leq \sum_{\omega_i} \frac{H^2}{\Lambda_{L_i+1}^{\omega_i}} \|\mathbf{w}\|_{2,\omega_i}^2,
 \end{aligned}$$

$$\begin{aligned}
 (3.35) \quad &\sum_{K \in \mathcal{T}^H} \sum_{y_i \in K} \left(\left\| \mathbf{u} - (\mathcal{I}_{L_i}^{\omega_i} \mathbf{w})_u \right\|_{L_a,K} + \left\| \theta - (\mathcal{I}_{L_i}^{\omega_i} \mathbf{w})_\theta \right\|_{L_d,K} \right) \\
 &= \sum_{\omega_i} \left(\left\| \mathbf{u} - (\mathcal{I}_{L_i}^{\omega_i} \mathbf{w})_u \right\|_{L_a,\omega_i} + \left\| \theta - (\mathcal{I}_{L_i}^{\omega_i} \mathbf{w})_\theta \right\|_{L_d,\omega_i} \right) \\
 &= \sum_{\omega_i} \|\mathbf{w} - \mathcal{I}_{L_i}^{\omega_i} \mathbf{w}\|_{0,\omega_i}^2 \leq \sum_{\omega_i} \frac{H^4}{(\Lambda_{L+1}^{\omega_i})^2} \|\mathbf{w}\|_{2,\omega_i}^2.
 \end{aligned}$$

Then combining the summation of Eq. (3.20) for all $K \in \mathcal{T}_H$ with Eq. (3.34) and Eq. (3.35), the proof is complete.

3.2. Steady state case. Some results for the prior error estimate of problem (2.1) will be firstly given in steady state case. For $\bar{\mathbf{u}} \in V_u(\Omega)$ and $\bar{\theta} \in V_\theta(\Omega)$, it follows that

$$(3.36) \quad \begin{aligned} a(\bar{\mathbf{u}}, \mathbf{v}_u) - b(\mathbf{v}_u, \bar{\theta}) &= \langle \bar{\mathbf{f}}, \mathbf{v}_u \rangle_a, \quad \forall \mathbf{v}_u \in V_u, \\ d(\bar{\theta}, v_\theta) &= \langle \bar{g}, v_\theta \rangle_d, \quad \forall v_\theta \in V_\theta. \end{aligned}$$

Define $V_{uH} = \text{span} \{ \Phi_{lu}^{\omega_i} \}$ and $V_{\theta H} = \text{span} \{ \Phi_{l\theta}^{\omega_i} \}$, where $\Phi_l^{\omega_i}(x) = (\Phi_{lu}^{\omega_i}(x), \Phi_{l\theta}^{\omega_i}(x))$, ($1 \leq i \leq N_v, 1 \leq l \leq L_i$). The discretization form of Eq. (3.36) is given as

$$(3.37) \quad \begin{aligned} a(\bar{\mathbf{u}}_H, \mathbf{v}_{uH}) - b(\mathbf{v}_{uH}, \bar{\theta}_H) &= \langle \bar{\mathbf{f}}, \mathbf{v}_{uH} \rangle_a, \quad \forall \mathbf{v}_{uH} \in V_{uH}, \\ d(\bar{\theta}_H, v_{\theta H}) &= \langle \bar{g}, v_{\theta H} \rangle_d, \quad \forall v_{\theta H} \in V_{\theta H}. \end{aligned}$$

Then for all $\mathbf{w} = (\mathbf{u}, \theta) \in V_u \times V_\theta$, define the Riesz projection operator $\mathcal{R}_H : V_u \times V_\theta \rightarrow V_{uH} \times V_{\theta H}$, and $\mathcal{R}_H = (\mathcal{R}_{Hu}(\mathbf{u}, \theta), \mathcal{R}_{H\theta}(\theta))$, we have

$$(3.38) \quad \begin{aligned} a(\mathbf{u} - \mathcal{R}_{Hu}(\mathbf{u}, \theta), \mathbf{v}_{uH}) - b(\mathbf{v}_{uH}, \theta - \mathcal{R}_{H\theta}(\theta)) &= 0, \quad \forall \mathbf{v}_{uH} \in V_{uH}, \\ d(\theta - \mathcal{R}_{H\theta}(\theta), v_{\theta H}) &= 0, \quad \forall v_{\theta H} \in V_{\theta H}. \end{aligned}$$

The following Lemma can be given with the similar method in [19].

LEMMA 3.4. For all $\mathbf{w} = (\mathbf{u}, \theta) \in V_u \times V_\theta$, and the definition of \mathcal{R}_H , we have

$$(3.39) \quad \|\mathbf{u} - \mathcal{R}_{Hu}(\mathbf{u}, \theta)\|_a \leq \inf_{\mathbf{v}_{uH} \in V_{uH}} \|\mathbf{u} - \mathbf{v}_{uH}\|_a + C_0 \|\theta - \mathcal{R}_{H\theta}(\theta)\|_c,$$

$$(3.40) \quad \|\theta - \mathcal{R}_{H\theta}(\theta)\|_d \leq \inf_{v_{\theta H} \in V_{\theta H}} \|\theta - v_{\theta H}\|_d.$$

LEMMA 3.5. For all $r \in L_d$, and let $\phi \in V_\theta$ be the solution of the dual problem $d(\phi, v_d) = c(r, v_\theta), \forall v_\theta \in V_\theta$, and $\phi_H \in V_{\theta H}$ be the solution of the discrete problem $d(\phi_H, v_\theta) = c(r, v_\theta), \forall v_\theta \in V_{\theta H}$. There holds

$$(3.41) \quad \|\phi - \phi_H\|_d \leq C_4 \|r\|_c.$$

where $C_4 = C_p^{\frac{1}{2}} \kappa_{min}^{-\frac{1}{2}}$, and C_p is the Poincaré constant.

PROOF. One can firstly estimate the following equations,

$$(3.42) \quad \|\phi - \phi_H\|_d^2 = d(\phi, \phi - \phi_H) = c(r, \phi - \phi_H) \leq \|r\|_c \|\phi - \phi_H\|_c.$$

$$(3.43) \quad C_p^{-1} \kappa_{min} \|\phi - \phi_H\|_c^2 \leq \kappa_{min} \|\nabla(\phi - \phi_H)\|_c^2 \leq \|\phi - \phi_H\|_d^2.$$

Combining Eq. (3.42) with Eq. (3.43), it follows that

$$(3.44) \quad \|\phi - \phi_H\|_d^2 \leq C_p^{\frac{1}{2}} \kappa_{min}^{-\frac{1}{2}} \|r\|_c \|\phi - \phi_H\|_d.$$

LEMMA 3.6. For all $\mathbf{w} = (\mathbf{u}, \theta) \in V_u \times V_\theta$, and the definition of \mathcal{R}_H , we have

$$(3.45) \quad \|\mathbf{u} - \mathcal{R}_{Hu}(\mathbf{u}, \theta)\|_a \leq \max\{1, C_4 C_0\} C(H, \Lambda_{L+1}^{\omega_i}) \|\mathbf{w}\|_{2, \Omega},$$

$$(3.46) \quad \|\theta - \mathcal{R}_{H\theta}(\theta)\|_d \leq C(H, \Lambda_{L+1}^{\omega_i}) \|\mathbf{w}\|_{2, \Omega},$$

$$(3.47) \quad \|\theta - \mathcal{R}_{H\theta}(\theta)\|_c \leq C_4 C(H, \Lambda_{L+1}) \|\mathbf{w}\|_{2, \Omega}.$$

where $C(H, \Lambda_{L+1}) = \left[C_2 \frac{H^2}{\Lambda_{L+1}} + (2C_1^2 H^2 + C_3 H^4) \frac{1}{(\Lambda_{L+1})^2} \right]^{\frac{1}{2}}$, and

$$\|\mathbf{w}\|_{s, \Omega}^2 = \sum_{\omega_i \in \Omega} \|\mathbf{w}\|_{s, \omega_i}^2.$$

PROOF. For all $\theta \in V_\theta$, and let $r := \theta - \mathcal{R}_{Hd}(\theta)$, it follows

$$(3.48) \quad \begin{aligned} \|\theta - \mathcal{R}_{H\theta}(\theta)\|_c^2 &= c(r, r) = d(\phi, r) = d(\phi - \phi_H, r) \\ &\leq \|\phi - \phi_H\|_d \|r\|_d \leq C_4 \|r\|_c \|r\|_d. \end{aligned}$$

Then we have

$$(3.49) \quad \|\theta - \mathcal{R}_{H,d}(\theta)\|_c \leq C_4 \|\theta - \mathcal{R}_{H,d}(\theta)\|_d.$$

Moreover, combining (3.39) with (3.49), it follows

$$(3.50) \quad \|\mathbf{u} - \mathcal{R}_{Hu}(\mathbf{u}, \theta)\|_a \leq \inf_{\mathbf{v}_{uH} \in V_{uH}} \|\mathbf{u} - \mathbf{v}_{uH}\|_a + C_4 C_0 \inf_{v_{\theta H} \in V_{\theta H}} \|\theta - v_{\theta H}\|_d.$$

By the definition of $\|\mathbf{w}\|_{s,\Omega}^2$, the proof is complete.

3.3. The prior error estimate of CGMsFEM. For \mathbf{f} and g in problem (2.1), we have

$$(3.51) \quad \langle \tilde{\mathbf{f}}, v_u \rangle_a = \langle \mathbf{f}, v_u \rangle, \forall v_u \in V_u, \quad \langle \tilde{g}, v_\theta \rangle_d = \langle g, v_\theta \rangle, \forall v_\theta \in V_\theta.$$

where $\tilde{\mathbf{f}} \in V_u$ and $\tilde{g} \in V_\theta$. Define

$$(3.52) \quad C^n(\mathbf{f}, g) = \frac{1}{2} \|\tilde{\mathbf{f}}^n - \tilde{\mathbf{f}}_H^n\|_a^2 + \tau_n \|\tilde{g}^n - \tilde{g}_H^n\|_d^2, \quad \forall n \in 1, \dots, N_T.$$

For simplicity of notation, let

$$(3.53) \quad C_1^n(\mathbf{w}) = 4C_4^2 (C_4^2 + C_0^2 \max\{1, C_4^2 C_0^2\}) \|\partial_t \mathbf{w}\|_{L^\infty(T_n, \|\cdot\|_{2,\Omega})},$$

$$(3.54) \quad C_2^n(\mathbf{w}) = 2C_4^2 \left(\|\partial_{tt} \theta\|_{L^\infty(T_n, \|\cdot\|_c)} + C_0^2 \|\partial_{tt} \mathbf{u}\|_{L^\infty(T_n, \|\cdot\|_a)} \right).$$

Then we have the following the prior error estimate of CGMsFEM.

THEOREM 3.2. Let $\mathbf{w} = (\mathbf{u}, \theta)$ and $\mathbf{w}_H = (\mathbf{u}_H, \theta_H)$ be the unique solution and CGMsFEM solution of problem (2.1), there holds

$$(3.55) \quad \begin{aligned} \frac{1}{4} \|\mathbf{u}^n - \mathbf{u}_H^n\|_a^2 + \frac{1}{4} \|\theta^n - \theta_H^n\|_c^2 &\leq \sum_{m=1}^n [C^m(\mathbf{f}, g) + \tau_m C^2(H, \Lambda_{L+1}) C_1^m(\mathbf{w}) \\ &\quad + \tau_m^3 C_2^m(\mathbf{w})] + \frac{1}{2} (C_4^2 + \max\{1, C_4^2 C_0^2\}) C^2(H, \Lambda_{L+1}) \|\mathbf{w}^n\|_{2,\Omega}^2, \end{aligned}$$

and

$$(3.56) \quad \begin{aligned} \sum_{m=1}^n \frac{1}{8} \tau_m \|\theta^m - \theta_H^m\|_d^2 &\leq \sum_{m=1}^n [C^m(\mathbf{f}, g) + \tau_m C^2(H, \Lambda_{L+1}) C_1^m(\mathbf{w}) \\ &\quad + \tau_m^3 C_2^m(\mathbf{w})] + \sum_{m=1}^n \frac{1}{4} \tau_m C^2(H, \Lambda_{L+1}) \|\mathbf{w}^n\|_{2,\Omega}^2. \end{aligned}$$

where $n \in \{1, 2, \dots, N_T\}$.

PROOF. By the definition of Riesz projection operator \mathcal{R}_H , and we define

$$(3.57) \quad \eta_{Hu}^n = \mathcal{R}_{Hu}(\mathbf{u}^n, \theta^n) - \mathbf{u}_H^n, \quad \eta_{H\theta}^n = \mathcal{R}_{H\theta}(\theta^n) - \theta_H^n.$$

Combining Eq. (2.12), we have

$$\begin{aligned} a(\eta_{Hu}^n, \mathbf{v}_{uH}) - b(\mathbf{v}_{uH}, \eta_{H\theta}^n) + c(\eta_{H\theta}^n - \eta_{H\theta}^{n-1}, v_{\theta H}) + b(\eta_{Hu}^n - \eta_{Hu}^{n-1}, v_{\theta H}) \\ + \tau_n d(\eta_{H\theta}^n, v_{\theta H}) = \langle \tilde{\mathbf{f}}^n - \tilde{\mathbf{f}}_H^n, \mathbf{v}_{uH} \rangle_a + \tau_n \langle \tilde{g}^n - \tilde{g}_H^n, v_{\theta H} \rangle_d \\ + c(\delta_{H\theta}^n, v_{\theta H}) + b(\delta_{Hu}^n, v_{\theta H}), \quad \forall (\mathbf{v}_{uH}, v_{\theta H}) \in V_{CGM} \end{aligned}$$

where

$$\begin{aligned} \delta_{H\theta}^n &= \mathcal{R}_{H\theta}(\theta^n) - \mathcal{R}_{H\theta}(\theta^{n-1}) - \tau_n \partial_t \theta^n \\ \delta_{Hu}^n &= \mathcal{R}_{Hu}(\mathbf{u}^n, \theta^n) - \mathcal{R}_{Hu}(\mathbf{u}^{n-1}, \theta^{n-1}) - \tau_n \partial_t \mathbf{u}^n. \end{aligned}$$

Define $v_{uH} = \eta_{Hu}^n - \eta_{Hu}^{n-1} \in V_{uH}$ and $v_{\theta H} = \eta_{H\theta}^n$, it follows

$$\begin{aligned} (3.58) \quad \frac{1}{2} \|\eta_{Hu}^n\|_a^2 + \frac{1}{2} \|\eta_{Hu}^n - \eta_{Hu}^{n-1}\|_a^2 + \frac{1}{2} \|\eta_{H\theta}^n\|_c^2 + \frac{1}{2} \|\eta_{H\theta}^n - \eta_{H\theta}^{n-1}\|_c^2 + \tau_n \|\eta_{Hd\theta}^n\|_d^2 \\ = \frac{1}{2} \|\eta_{Hu}^{n-1}\|_a^2 + \frac{1}{2} \|\eta_{H\theta}^{n-1}\|_c^2 + \langle \tilde{\mathbf{f}}^n - \tilde{\mathbf{f}}_H^n, \eta_{Hu}^n - \eta_{Hu}^{n-1} \rangle_a \\ + \tau_n \langle \tilde{g}^n - \tilde{g}_H^n, \eta_{H\theta}^n \rangle_d + c(\delta_{H\theta}^n, \eta_{H\theta}^n) + b(\delta_{Hu}^n, \eta_{Hu}^n). \end{aligned}$$

Similar to Eq. (3.43), by use of $\|\eta_{H\theta}^n\|_c \leq C_4 \|\eta_{H\theta}^n\|_d$, we have

$$\begin{aligned} (3.59) \quad \frac{1}{2} \|\eta_{Hu}^n\|_a^2 + \frac{1}{2} \|\eta_{H\theta}^n\|_c^2 + \frac{1}{4} \tau_n \|\eta_{H\theta}^n\|_d^2 \leq \frac{1}{2} \|\eta_{Hu}^{n-1}\|_a^2 + \frac{1}{2} \|\eta_{H\theta}^{n-1}\|_c^2 + C^n(\mathbf{f}, g) \\ + 4C_4^2 \tau_n^{-1} \|\delta_{H\theta}^n\|_c^2 + 4C_4^2 \tau_n^{-1} C_0^2 \|\delta_{Hu}^n\|_a^2. \end{aligned}$$

Based on the regularity assumption of problem and Eq. (3.47), we have

$$\begin{aligned} (3.60) \quad \|\delta_{H\theta}^n\|_c = \left\| - \int_{T_n} [\partial_t \theta(s) - \mathcal{R}_{H\theta}(\partial_t \theta(s))] ds - \int_{T_n} (s - t_{n-1}) \partial_{tt} \theta(s) dt \right\|_c \\ \leq \tau_n C_4 C(H, \Lambda_{L+1}) \|\partial_t \mathbf{w}\|_{L^\infty(T_n, \|\cdot\|_{2,\Omega})} + \frac{1}{2} \tau_n^2 \|\partial_{tt} \theta\|_{L^\infty(T_n, \|\cdot\|_c)}. \end{aligned}$$

Similarly, using Eq. (3.45), we obtain

$$(3.61) \quad \|\delta_{Hu}^n\|_a \leq \tau_n \max\{1, C_4 C_0\} C(H, \Lambda_{L+1}) \|(\partial_t \mathbf{w})\|_{L^\infty(T_n, \|\cdot\|_{2,\Omega})} + \frac{1}{2} \tau_n^2 \|\partial_{tt} \mathbf{u}\|_{L^\infty(T_n, \|\cdot\|_a)}.$$

Combining Eq. (3.60) with Eq. (3.61), it follows

$$(3.62) \quad 4C_4^2 \tau_n^{-1} \|\delta_{H\theta}^n\|_c^2 + 4C_4^2 \tau_n^{-1} C_0^2 \|\delta_{Hu}^n\|_a^2 \leq \tau_n C^2(H, \Lambda_{L+1}) C_1^n(\mathbf{w}) + \tau_n^3 C_2^n(\mathbf{w}).$$

Let $u_H^0 = \mathcal{R}_{Hu}(\mathbf{u}^0, \theta^0)$ and $\theta_H^0 = \mathcal{R}_{H\theta}(\theta^0)$, then $\eta_{Hu}^0 = 0$ and $\eta_{H\theta}^0 = 0$, we have

$$\begin{aligned} (3.63) \quad \frac{1}{2} \|\eta_{Hu}^n\|_a^2 + \frac{1}{2} \|\eta_{H\theta}^n\|_c^2 + \sum_{m=1}^n \frac{1}{4} \tau_m \|\eta_{H\theta}^m\|_d^2 \leq \sum_{m=1}^n [C^m(\mathbf{f}, g) \\ + \tau_m C^2(H, \Lambda_{L+1}) C_1^m(\mathbf{w}) + \tau_m^3 C_2^m(\mathbf{w})]. \end{aligned}$$

Finally, the proof is complete by using the triangle inequality.

4. Numerical experiments. In this section, we present several numerical examples to evaluate the performance of the proposed CGMsFEM for the thermomechanical problem (2.1), and mainly focus on the verification of the accuracy and efficiency of CGMsFEM. The computation domain is $\Omega = [0, 1]^2$ and time interval is $(0, 1]$. The Dirichlet condition and Neumann boundary conditions for the displacement and temperature fields are defined as 0 in $\Gamma_D^u = \Gamma_D^\theta = [0, 1] \times 0$ and $\Gamma_N^u = \Gamma_N^\theta = \partial\Omega \setminus \Gamma_D^u$, respectively. The solutions $(\mathbf{u}^{cgm}, \theta^{cgm})$ of CGMsFEM will be compared with the reference solutions $(\mathbf{u}^{ref}, \theta^{ref})$ of standard finite element method and solutions $(\mathbf{u}^{gm}, \theta^{gm})$ of GMsFEM. Then based on Theorem 3.2, the relative energy errors of each solutions and the total relative energy errors are defined as follows

$$(4.1) \quad \begin{aligned} \|E_u\|_e &= \frac{\left(\int_{\Omega} \sigma(E_u) : \epsilon(E_u) dx \right)^{\frac{1}{2}}}{\left(\int_{\Omega} \sigma(\mathbf{u}) : \epsilon(\mathbf{u}) dx \right)^{\frac{1}{2}}}, \quad \|E_\theta\|_e = \frac{\left(\int_{\Omega} \kappa \nabla E_\theta \cdot \nabla E_\theta dx \right)^{\frac{1}{2}}}{\left(\int_{\Omega} \kappa \nabla \theta \cdot \nabla \theta dx \right)^{\frac{1}{2}}}, \\ \|E_w\|_e &= \frac{\left(\int_{\Omega} \sigma(E_u) : \epsilon(E_u) + \kappa \nabla E_\theta \cdot \nabla E_\theta dx \right)^{\frac{1}{2}}}{\left(\int_{\Omega} \sigma(\mathbf{u}) : \epsilon(\mathbf{u}) + \kappa \nabla \theta \cdot \nabla \theta dx \right)^{\frac{1}{2}}}, \end{aligned}$$

where E_u represents the energy error $E_u^{cgm} = \mathbf{u}^{cgm} - \mathbf{u}^{ref}$ or $E_u^{gm} = \mathbf{u}^{gm} - \mathbf{u}^{ref}$, and E_θ denotes the energy error $E_\theta^{cgm} = \theta^{cgm} - \theta^{ref}$ or $E_\theta^{gm} = \theta^{gm} - \theta^{ref}$. Our numerical experiments are performed on a desktop workstation with 16G memory and a 3.4GHz Core i7 CPU.

4.1. Verification of CGMsFEM with periodic microstructure. In this example, the efficiency and accuracy of CGMsFEM is verified for heterogeneous media with periodic microstructure. The body force \mathbf{f} and heat source g are chosen as

$$\mathbf{f}(x, y) = 0, \quad g(x, y) = 10.$$

The initial boundary condition is defined as

$$\theta_0(x, y) = 500x(1-x)y(1-y).$$

Then the Lamé coefficients μ, λ , thermal conductivity coefficient κ , and expansion coefficient β are showed in Figure 4.1, where the contrasts are chosen as $\lambda_{\max} : \lambda_{\min} = 10^2 : 1$, $\mu_{\max} : \mu_{\min} = 10^2 : 1$, $\kappa_{\max} : \kappa_{\min} = 10^4 : 1$, $\beta_{\max} : \beta_{\min} = 10^4 : 1$. The corresponding relaxation coefficients $\gamma_1 = 0.4, \gamma_2 = 0.04$ are given, and the time step is $\tau = 0.02$. Here, the 200×200 fine grid is used for reference solution, and 20×20 coarse grid for the proposed CGMsFEM and GMsFEM. The number of local coupling multiscale basis functions for CGMsFEM are fixed to 8, and the total number of GMsFEM multiscale basis functions for displacement \mathbf{u} and θ are also chosen as 8.

Figure 4.2 demonstrates the contour plots of reference solutions $(\mathbf{u}^{ref}, \theta^{ref})$, CGMsFEM solutions $(\mathbf{u}^{cgm}, \theta^{cgm})$, and GMsFEM solutions $(\mathbf{u}^{gm}, \theta^{gm})$, and it can be concluded that the proposed CGMsFEM has higher accuracy than GMsFEM with the same number of multiscale basis functions. For the comparison purpose, we calculate the energy error of CGMsFEM and GMsFEM defined by the equation (4.1). The numerical results for different number $L = 4, 6, \dots, 16$ of multiscale basis functions

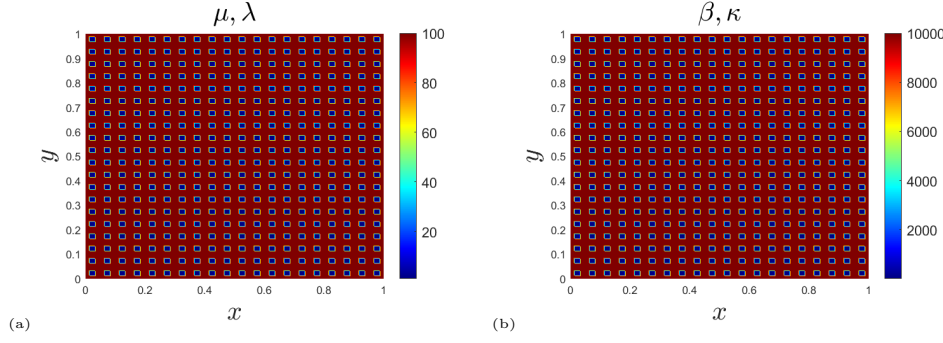


FIG. 4.1. Contour plots of the material coefficients in periodic microstructure. (a) Lamé coefficients μ , and λ ; (b) Thermal conductivity coefficient κ , and expansion coefficient β .

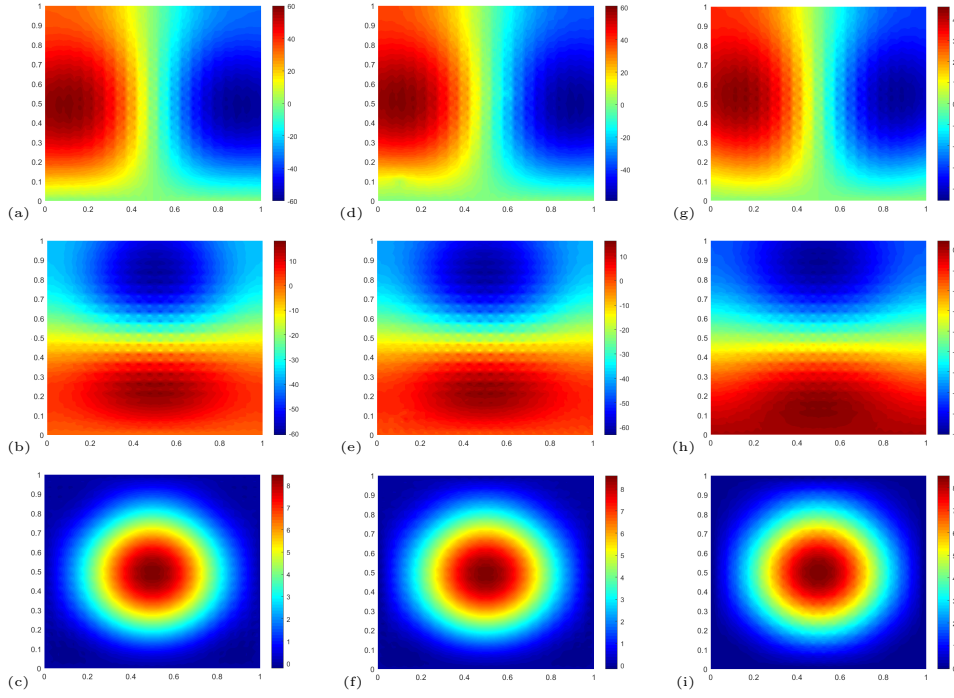


FIG. 4.2. Contour plots of solutions for periodic microstructure. The reference solutions: (a) u_1^{ref} (b) u_2^{ref} and (c) θ^{ref} ; The CGMsFEM solutions: (d) u_1^{cgm} (e) u_2^{cgm} and (f) θ^{cgm} ; The GMSFEM solutions: (g) u_1^{gm} (h) u_2^{gm} and (i) θ^{gm} .

are given in Table 4.1. From the table we observe that the total relative energy error $\|E_w^{cgm}\|_e$ for CGMsFEM decrease as L increases, and the similar results can also be showed for the energy errors $\|E_\theta^{cgm}\|_e$ and $\|E_u^{cgm}\|_e$. Moreover, by taking GMSFEM as reference, it can also clearly be found that the energy errors of CGMsFEM with $L = 4$ are obviously smaller than that of GMSFEM with $L = 16$ in Figure 4.3, which demonstrate that the proposed CGMsFEM is more efficient than GMSFEM.

TABLE 4.1
Comparison of energy errors for CGMsFEM and GMsFEM

L	Eigvalue	$\ E_\theta^{cgm}\ _e$	$\ E_\theta^{gm}\ _e$	$\ E_u^{cgm}\ _e$	$\ E_u^{gm}\ _e$	$\ E_w^{cgm}\ _e$	$\ E_w^{gm}\ _e$
4	14.80	0.1630	0.4611	0.2048	0.3226	0.1922	0.3734
6	35.56	0.1316	0.4221	0.1687	0.2914	0.1576	0.3395
8	37.54	0.1275	0.4212	0.1420	0.2897	0.1374	0.3382
10	40.86	0.0793	0.4045	0.0790	0.2325	0.0791	0.2995
12	43.65	0.0687	0.3972	0.0728	0.2134	0.0715	0.2865
14	70.87	0.0634	0.3880	0.0543	0.2046	0.0574	0.2779
16	77.68	0.0590	0.3785	0.0383	0.1768	0.0461	0.2602

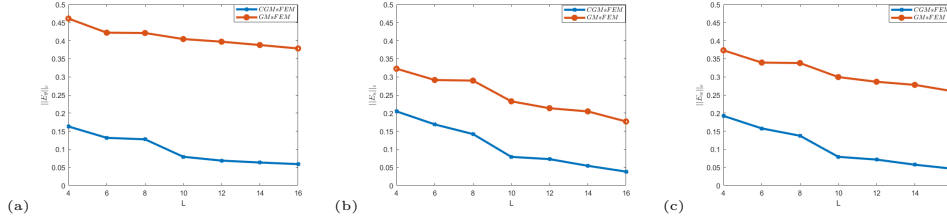


FIG. 4.3. Comparison of relative energy errors of the CGMsFEM and GMsFEM in periodic microstructure. (a) E_θ (b) E_u , and (c) E_w ;

4.2. Application to random microstructure and material coefficients.

In order to validate the good applicability of CGMsFEM, two kinds of tests (Test A, B) are performed in this subsection. In test A, heterogeneous media have random microstructure and deterministic coefficients, and in test B, both the microstructure and coefficients of materials are random.

Test A: *Heterogeneous media with random microstructure and deterministic coefficients.* In this simulation, the body force \mathbf{f} and heat source g are chosen as

$$\mathbf{f}(x, y) = \mathbf{0}, \quad g(x, y) = 10 \times \exp\left(-\frac{(x-0.2)^2 + (y-0.4)^2}{2 \times 0.2^2}\right).$$

The initial boundary conditon is defined as

$$\theta_0(x, y) = \cos(\pi x)\cos(\pi y) + 1.5.$$

Then the Lamé coefficients μ , λ , Conductivity coefficient κ , and thermal expansion coefficient β are showed in the left of Figure 4.4, where the contrasts are chosen as $\lambda_{\max} : \lambda_{\min} = 10^2 : 1$, $\mu_{\max} : \mu_{\min} = 10^2 : 1$, $\kappa_{\max} : \kappa_{\min} = 10^3 : 1$, $\beta_{\max} : \beta_{\min} = 5.0 \times 10^4 : 1$. The corresponding relaxation coefficients $\gamma_1 = 0.75$, $\gamma_2 = 7.0 \times 10^{-2}$ are given, and the time step is $\tau = 0.01$. Here, the 100×100 fine grid is used for reference solution, and 10×10 coarse grid for the proposed CGMsFEM and GMsFEM. The number of local coupling multiscale basis functions for CGMsFEM are fixed to 10, and the total number of local GMsFEM multiscale basis functions for displacement \mathbf{u} and θ are also chosen as 10.

Test B: *Heterogeneous media with random microstructure and coefficients.* In this test, the initial conditions, boundary conditions and source terms are the same as in subsection 4.1. The material coefficients $\kappa(\mathbf{x}; \xi)$, $\lambda(\mathbf{x}; \xi)$, $\mu(\mathbf{x}; \xi)$ and $\beta(\mathbf{x}; \xi)$ satisfy the following logarithmic Gaussian random field

$$(4.2) \quad \exp\left(\mathcal{GP}(b_0(\mathbf{x}), \text{Cov}(\mathbf{x}_1, \mathbf{x}_2))\right),$$

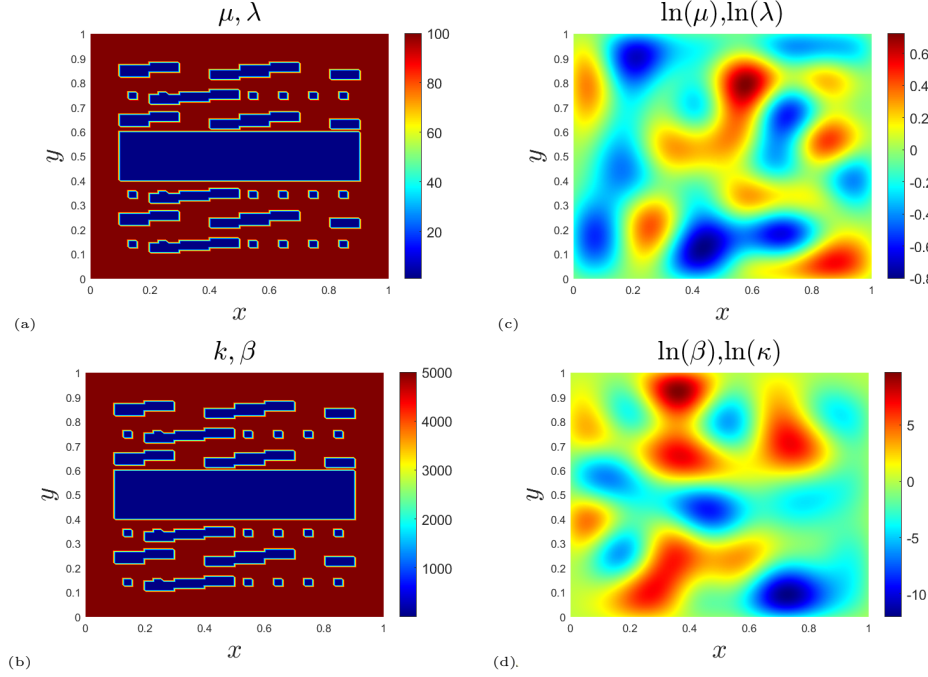


FIG. 4.4. Contour plots of one sample for the material coefficients. Lamé coefficients μ , and λ : (a) Test A and (c) Test B ; Thermal conductivity coefficient κ , and expansion coefficient β : (b) Test A and (d) Test B .

where $\text{Cov}(\mathbf{x}_1, \mathbf{x}_2) = \sigma^2 \exp(-\|\mathbf{x}_1 - \mathbf{x}_2\|^2/l^2)$, x_1 and x_2 are spatial coordinates in Ω , σ^2 is the overall variance, and l is the length scale. Then we take $l = 0.01, \sigma = 10, b_0(x) = 0$ for $\kappa(\mathbf{x}; \xi)$, $\beta(\mathbf{x}; \xi)$, and $l = 0.01, \sigma = 10, b_0(x) = 0$ for $\lambda(\mathbf{x}; \xi)$, $\mu(\mathbf{x}; \xi)$. For simplicity, the samples are obtained by the help of Karhunen-Loève expansion (KLE) with 50 truncated terms. The right parts of Figure 4.4 show one sample of $\kappa(\mathbf{x}; \xi)$, $\lambda(\mathbf{x}; \xi)$, $\mu(\mathbf{x}; \xi)$ and $\beta(\mathbf{x}; \xi)$. Let time step size be $\tau_n = 0.01$. Fine grid size $h = \frac{1}{100}$, coarse grid size $H = \frac{1}{10}$ and relaxation coefficients $\gamma_1 = 0.7, \gamma_2 = 8.0 \times 10^{-6}$ are used for simulation. The number of local coupling multiscale basis functions for CGMsFEM are fixed to 8, and the total number of local GMsFEM multiscale basis functions for displacement \mathbf{u} and θ are also chosen as 8.

TABLE 4.2

Test A: Relative energy errors of the CGMsFEM and GMsFEM with different contrast ratio of β_{\max} and β_{\min} .

Ratio	$\ E_{\theta}^{cgm}\ _e$	$\ E_{\theta}^{gm}\ _e$	$\ E_u^{cgm}\ _e$	$\ E_u^{gm}\ _e$	$\ E_w^{cgm}\ _e$	$\ E_w^{gm}\ _e$
1×10^1	0.0474	0.0946	0.0838	0.2682	0.0474	0.0947
1×10^2	0.0638	0.0946	0.1197	0.2538	0.0638	0.0947
1×10^3	0.0805	0.1647	0.1364	0.5539	0.0822	0.1828
5×10^3	0.1306	0.8367	0.1311	0.7455	0.1308	0.7926
1×10^4	0.1512	0.5599	0.1519	0.5171	0.1512	0.5360

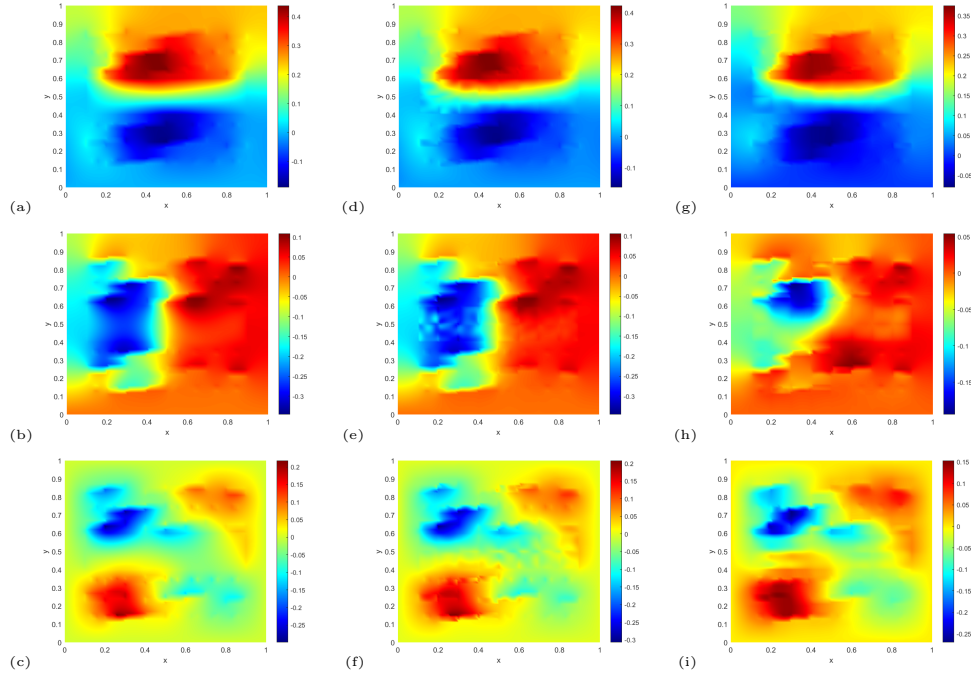


FIG. 4.5. Contour plots of solutions for Test A. The reference solutions: (a) u_1^{ref} (b) u_2^{ref} and (c) θ^{ref} ; The CGMsFEM solutions: (d) u_1^{cgm} (e) u_2^{cgm} and (f) θ^{cgm} ; The GMsFEM solutions: (g) u_1^{gm} (h) u_2^{gm} and (i) θ^{gm} .

TABLE 4.3

Test B: Relative energy errors of the CGMsFEM and GMsFEM with different variance σ of β .

σ	$\ E_{\theta}^{cgm}\ _e$	$\ E_{\theta}^{gm}\ _e$	$\ E_u^{cgm}\ _e$	$\ E_u^{gm}\ _e$	$\ E_w^{cgm}\ _e$	$\ E_w^{gm}\ _e$
2	0.2075	0.3259	0.2124	0.2916	0.0474	0.0947
3	0.2336	0.3410	0.2478	0.2871	0.2072	0.3116
4	0.2739	0.4202	0.2119	0.2665	0.2371	0.3152
5	0.2656	0.4194	0.2135	0.2677	0.2225	0.3048
6	0.4144	0.5782	0.1492	0.2250	0.1781	0.2728

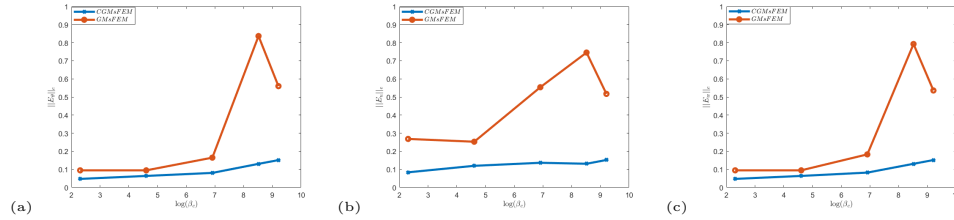


FIG. 4.7. Test A: Comparison of relative energy errors for the CGMsFEM and GMsFEM with different contrast ratio of β_{max} and β_{min} (a) E_{θ} (b) E_u , and (c) E_w , where $\beta_c = \frac{\beta_{max}}{\beta_{min}}$.

The reference solutions ($\mathbf{u}^{ref}, \theta^{ref}$), the CGMsFEM solutions ($\mathbf{u}^{cgm}, \theta^{cgm}$) and the GMsFEM solutions ($\mathbf{u}^{gm}, \theta^{gm}$) of Test A and Test B are presented in Figure 4.5

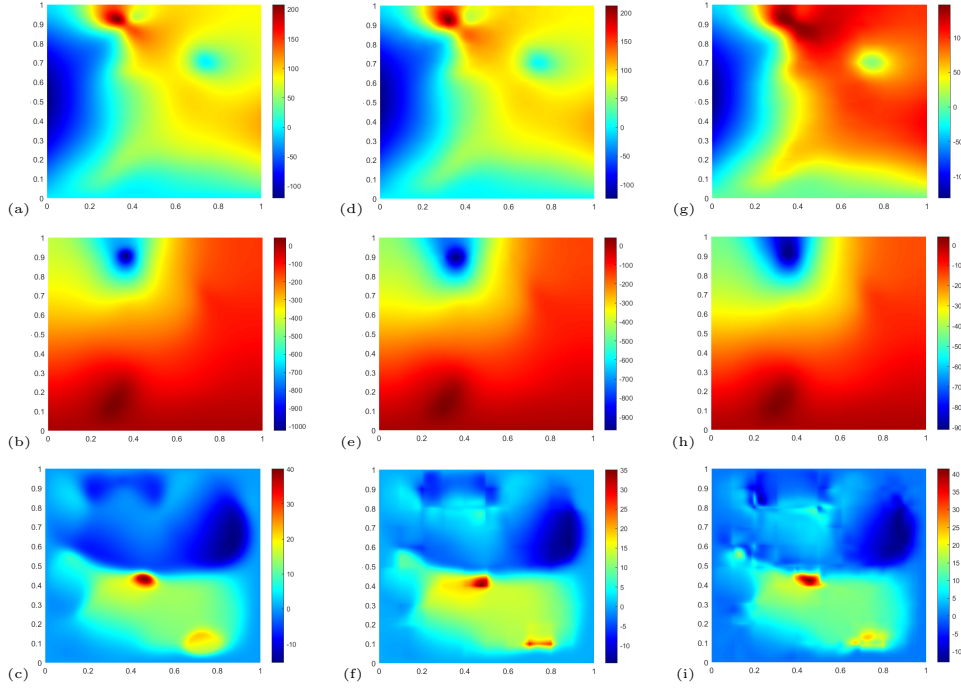


FIG. 4.6. Contour plots of solutions for Test B. The reference solutions: (a) u_1^{ref} (b) u_2^{ref} and (c) θ^{ref} ; The CGMsFEM solutions: (d) u_1^{cgm} (e) u_2^{cgm} and (f) θ^{cgm} ; The GMSFEM solutions: (g) u_1^{gm} (h) u_2^{gm} and (i) θ^{gm} .

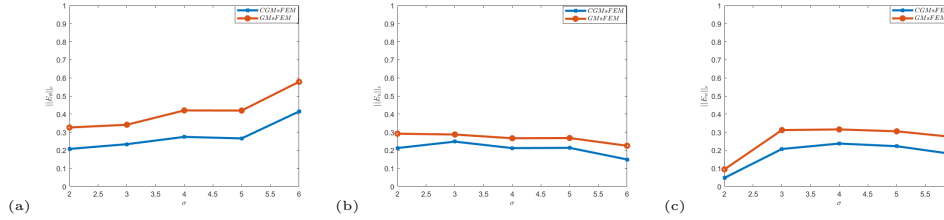


FIG. 4.8. Test B: Comparison of relative energy errors of the CGMsFEM and GMSFEM with different variance σ of β . (a) E_θ (b) E_u , and (c) E_w ;

and Figure 4.6, where the total number of samples are taken as 30 for each material coefficient in Test B, then the numerical expectation of solutions are given. It can be observed that the CGMsFEM solutions have higher accuracy than GMSFEM solutions by the reference solutions as comparison, which is consistent with the periodic case. Moreover, in order to explore the influence of different coefficients on the results, we compare the energy errors of the CGMsFEM and GMSFEM with the change of β . In Test A, the contrast ratio of β_{\max} and β_{\min} constantly varies, and in Test B, the variance σ is also constantly changed. Table 4.2 and Table 4.3 report the energy errors E_θ , E_u , and (c) E_w of the CGMsFEM and GMSFEM for Test A and Test B in detail. For more clearly demonstration, we also depict the trend of the energy errors with the contrast ratio of β_{\max} and β_{\min} in Figure 4.7 for Test A,

and with the variance σ of $\ln(\beta)$ in Figure 4.8 for Test B. For both of CGMsFEM and GMsFEM, we observe that the energy errors of the CGMsFEM are almost at the same level, while those of the GMsFEM change significantly. Although the whole system becomes extremely complex with increasing the contrast ratio or the variance of two material coefficients, the energy error of the whole system stays in a stable state, which is hardly affected by the complexity of system. This is also consistent with that in subsection 4.1. In addition, the accuracy of the CGMsFEM is always better than that of the GMsFEM for Test A and Test B even in the more complex case. Those numerical results demonstrate that the CGMsFEM is computationally quite efficient and accurate with the wide applicability in many scenarios.

5. Conclusions. In this paper, a novel CGMsFEM is proposed to efficiently simulate thermomechanical behaviors of heterogeneous media, which is suitable for both the weak and strong coupling setting. To the best of our knowledge, this paper is the first example of designed and analyzed coupling multiscale basis functions for GMsFEM of multiphysics problems. Two relaxation coefficients are innovative designed for local coupling spectral problems. The constructed multiscale basis functions can more accurately capture the multiphysical coupling information of the original thermomechanical problems, which obviously reduce the orders of global stiffness matrix. Moreover, the corresponding convergence analysis is derived in details, where the error of CGMsFEM is closely related to the eigenvalue decay in each local coarse block, and the upper error bound is independent of the two relaxation coefficients. Numerical experiments show that the proposed CGMsFEM is stable and effective, and can provide enough numerical accuracy, which support the theoretical results of this paper.

Despite a number of simplifying hypotheses adopted in this study, the CGMsFEM presented here is quite general, and provides a generalized framework to design the coupling basis functions for fully coupled multiphysics multiscale problems under the ultimate load. Future work will focus on the analysis of the optimal relaxation coefficients for solving the local coupling spectral problems, although we find that they can be flexibly chosen without affecting the efficiency and accuracy of CGMsFEM through numerical experiments.

Acknowledgments. The authors wish to thank Dr. Fan Chi for the strong personal support and helpful discussions in numerical experiments.

Appendix A. Eigenfunctions for CGMsFEM and GMsFEM in peridic microstructure. Figure A.1 demonstrates the different of eigenfunctions of the CGMsFEM and GMsFEM used in subsection 4.1. It can be observed that the first three or four eigenfunctions from the local coupling spectral problem of CGMsFEM can more accurately capture the microscopic oscillating information than that of GMsFEM, where less eigenfunctions are needed to represent the physical characteristics of microstructure for CGMsFEM.

REFERENCES

- [1] G. ALLAIRE, *Homogenization and Two-Scale Convergence*, SIAM Journal on Mathematical Analysis, 23 (1992), pp. 1482–1518.
- [2] I. BABUŠKA, R. LIPTON, P. SINZ, AND M. STUEBNER, *Multiscale-Spectral GFEM and optimal oversampling*, Computer Methods in Applied Mechanics and Engineering, 364 (2020), p. 112960.
- [3] I. BABUSKA AND J. OSBORN, *Generalized finite element methods: Their performance and their relation to mixed methods*, SIAM Journal on Numerical Analysis, 20 (1983), pp. 510–536.

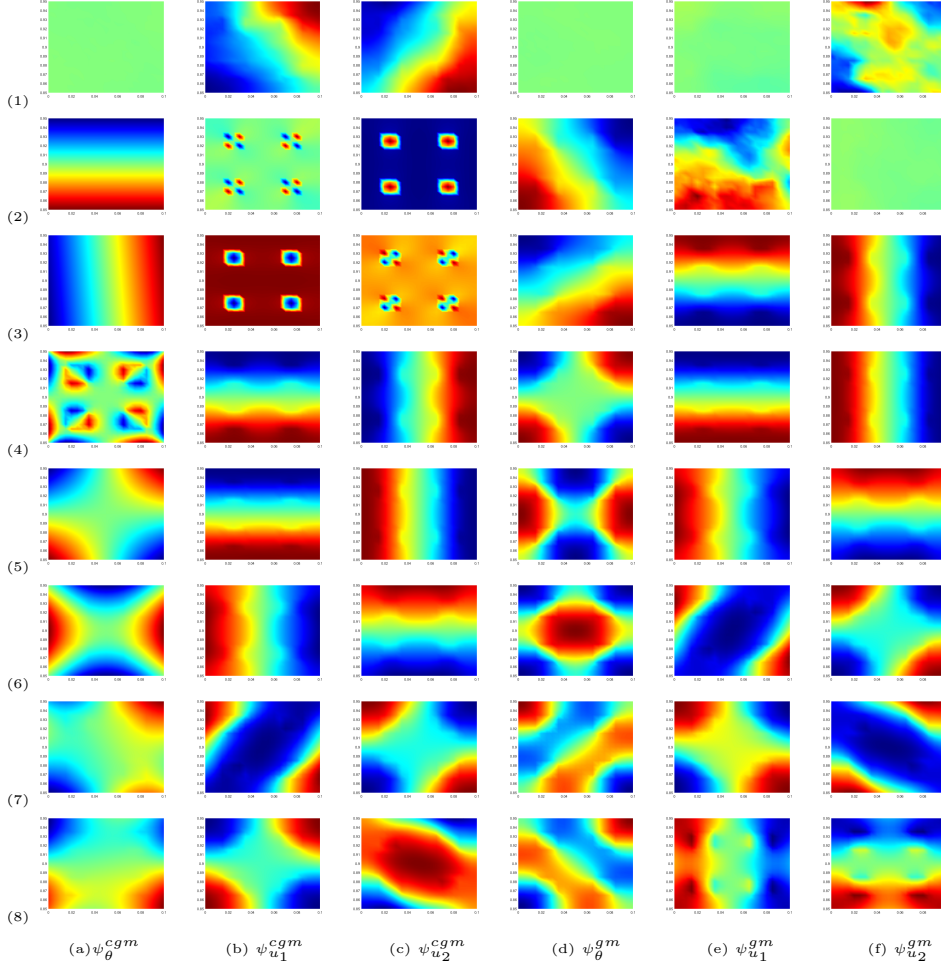


FIG. A.1. Contour plots of 8 eigenfunctions of the CGMsFEM and GMSFEM used in subsection 4.1. CGMsFEM: (a) ψ_θ^{cgm} (b) $\psi_{u_1}^{cgm}$ and (c) $\psi_{u_2}^{cgm}$; GMSFEM: (d) ψ_θ^{gm} (e) $\psi_{u_1}^{gm}$ and (f) $\psi_{u_2}^{gm}$;

- [4] A. BENSOUSSAN, J.-L. LIONS, AND G. PAPANICOLAOU, *Asymptotic Analysis for Periodic Structures*, Elsevier North-Holland, 1978.
- [5] R. BUTLER, T. DODWELL, A. REINARZ, A. SANDHU, R. SCHEICHL, AND L. SEELINGER, *High-performance dune modules for solving large-scale, strongly anisotropic elliptic problems with applications to aerospace composites*, Computer Physics Communications, 249 (2020), p. 106997.
- [6] J. P. CARTER AND J. R. BOOKER, *Finite element analysis of coupled thermoelasticity*, Computers & Structures, 31 (1989), pp. 73–80.
- [7] F. CHEN, E. CHUNG, AND L. JIANG, *Least-squares mixed generalized multiscale finite element method*, Computer Methods in Applied Mechanics and Engineering, 311 (2016), pp. 764–787.
- [8] R. CHIBA AND Y. SUGANO, *Optimisation of material composition of functionally graded materials based on multiscale thermoelastic analysis*, Acta Mechanica, 223 (2012), pp. 891–909.
- [9] E. T. CHUNG, Y. EFENDIEV, AND G. LI, *An adaptive GMSFEM for high-contrast flow problems*, Journal of Computational Physics, 273 (2014), pp. 54–76.
- [10] C. M. DAFERMOS, *On the existence and the asymptotic stability of solutions to the equations of linear thermoelasticity*, Archive For Rational Mechanics And Analysis, 29 (1968), pp. 241–271.

- [11] H. DONG, J. CUI, Y. NIE, Z. YANG, AND Z. YANG, *Multiscale computational method for heat conduction problems of composite structures with diverse periodic configurations in different subdomains*, Computers & Mathematics with Applications, 76 (2018), pp. 2549–2565.
- [12] H. DONG, Z. YANG, X. GUAN, AND J. CUI, *Stochastic higher-order three-scale strength prediction model for composite structures with micromechanical analysis*, Journal of Computational Physics, 465 (2022), p. 111352.
- [13] P. DUCHENE, S. CHAKI, A. AYADI, AND P. KRAWCZAK, *A review of non-destructive techniques used for mechanical damage assessment in polymer composites*, Journal of Materials Science, 53 (2018), pp. 7915–7938.
- [14] M. DUFLLOT, *The extended finite element method in thermoelastic fracture mechanics*, International Journal for Numerical Methods in Engineering, 74 (2008), pp. 827–847.
- [15] W. E, B. ENGQUIST, X. LI, W. REN, AND E. VANDEN-ELJNDEN, *Heterogeneous multiscale methods: A review*, Communications in Computational Physics, 2 (2007), pp. 367–450.
- [16] S. EBERLE, *FEM–BEM coupling for the thermoelastic wave equation with transparent boundary conditions in 3D*, Zeitschrift für angewandte Mathematik und Physik, 73 (2022), p. 163.
- [17] Y. EFENDIEV, J. GALVIS, AND T. Y. HOU, *Generalized multiscale finite element methods (GMS-FEM)*, Journal of Computational Physics, 251 (2013), pp. 116–135.
- [18] A. ENTEZARI, M. FILIPPI, AND E. CARRERA, *Unified finite element approach for generalized coupled thermoelastic analysis of 3D beam-type structures, part 1: Equations and formulation*, Journal of Thermal Stresses, 40 (2017), pp. 1386–1401.
- [19] A. ERN AND S. MEUNIER, *A posteriori error analysis of Euler-Galerkin approximations to coupled elliptic-parabolic problems*, ESAIM: Mathematical Modelling and Numerical Analysis - Modélisation Mathématique et Analyse Numérique, 43 (2009), pp. 353–375.
- [20] Y. FENG, M. DENG, J. CUI, AND X. GUAN, *A two-scale finite element analysis of the thermoelastic effects in composites*, International Journal of Computational Methods, 11 (2014), p. 1350066.
- [21] G. A. FRANCFORT, *Homogenization and Linear Thermoelasticity*, SIAM Journal on Mathematical Analysis, 14 (1983), pp. 696–708.
- [22] X. GUAN, L. JIANG, AND Y. WANG, *Multiscale model reduction for stochastic elasticity problems using ensemble variable-separated method*, Journal of Computational and Applied Mathematics, 421 (2023), p. 114895.
- [23] X. GUAN, H. YU, AND X. TIAN, *A stochastic second-order and two-scale thermo-mechanical model for strength prediction of concrete materials*, International Journal for Numerical Methods in Engineering, 108 (2016), pp. 885–901.
- [24] P. HENNING AND A. MÅLQVIST, *Localized Orthogonal Decomposition Techniques for Boundary Value Problems*, SIAM Journal on Scientific Computing, 36 (2014), pp. A1609–A1634.
- [25] T. HOU AND Y. EFENDIEV, *Multiscale Finite Element Methods: Theory and Applications*, Springer, New York, NY, 2009.
- [26] T. J. HUGHES, G. R. FEIJÓO, L. MAZZEI, AND J. B. QUINCY, *The variational multiscale method—a paradigm for computational mechanics*, Computer Methods in Applied Mechanics and Engineering, 166 (1998), pp. 3–24. Advances in Stabilized Methods in Computational Mechanics.
- [27] C. MA, R. SCHEICHL, AND T. DODWELL, *Novel Design and Analysis of Generalized Finite Element Methods Based on Locally Optimal Spectral Approximations*, SIAM Journal on Numerical Analysis, 60 (2022), pp. 244–273.
- [28] A. MÅLQVIST AND A. PERSSON, *A generalized finite element method for linear thermoelasticity*, ESAIM: Mathematical Modelling and Numerical Analysis, 51 (2017), pp. 1145–1171.
- [29] A. MÅLQVIST AND D. PETERSEIM, *Localization of elliptic multiscale problems*, Mathematics of Computation, 83 (2014), pp. 2583–2603.
- [30] W. H. NG, P. P. FRIEDMANN, AND A. M. WAAS, *Thermomechanical behavior of a damaged thermal protection system: Finite-element simulations*, Journal of Aerospace Engineering, 25 (2012), pp. 90–102.
- [31] I. ÖSZDEMİR, W. BREKELMANS, AND M. GEERS, *Fe² computational homogenization for the thermo-mechanical analysis of heterogeneous solids*, Computer Methods in Applied Mechanics and Engineering, 198 (2008), pp. 602–613.
- [32] P. PEDERSEN AND N. L. PEDERSEN, *Strength optimized designs of thermoelastic structures*, Structural and Multidisciplinary Optimization, 42 (2010), pp. 681–691.
- [33] S. PETER AND S. MEIR, *Existence of A Solution to The N Dimensional Problem of Thermoelastic Contact*, Communications in Partial Differential Equations, 17 (1992), pp. 1597–1618.
- [34] R. SHOWALTER, *Diffusion in Poro-Elastic Media*, Journal of Mathematical Analysis and Applications, 251 (2000), pp. 310–340.
- [35] N. STRÖMBERG, *Finite element treatment of two-dimensional thermoelastic wear problems*,

- Computer Methods in Applied Mechanics and Engineering, 177 (1999), pp. 441–455.
- [36] M. VASILYEVA AND D. STALNOV, *A Generalized Multiscale Finite Element Method for Thermoelasticity Problems*, in Numerical Analysis and Its Applications, Lecture Notes in Computer Science, Cham, 2017, Springer International Publishing, pp. 713–720.
 - [37] X. WANG, L. CAO, AND Y. WONG, *Multiscale Computation and Convergence for Coupled Thermoelastic System in Composite Materials*, Multiscale Modeling & Simulation, 13 (2015), pp. 661–690.
 - [38] H. C. YOON, K. K. VASUDEVA, AND S. M. MALLIKARJUNAIAH, *Finite element model for a coupled thermo-mechanical system in nonlinear strain-limiting thermoelastic body*, Communications in Nonlinear Science and Numerical Simulation, 108 (2022), p. 106262.
 - [39] A. ŽENÍŠEK, *Finite element methods for coupled thermoelasticity and coupled consolidation of clay*, RAIRO. Analyse numérique, 18 (1984), pp. 183–205.
 - [40] S. ZHANG, D. S. YANG, H. W. ZHANG, AND Y. G. ZHENG, *Coupling extended multiscale finite element method for thermoelastic analysis of heterogeneous multiphase materials*, Computers & Structures, 121 (2013), pp. 32–49.
 - [41] Y. ZHENG, H. ZHANG, J. LV, AND H. ZHANG, *An arbitrary multi-node extended multiscale finite element method for thermoelastic problems with polygonal microstructures*, International Journal of Mechanics and Materials in Design, 16 (2020), pp. 35–56.